iScience

CellPress

Article

Inositol 1,4,5-Trisphosphate Receptor Type 3 Regulates Neuronal Growth Cone Sensitivity to Guidance Signals

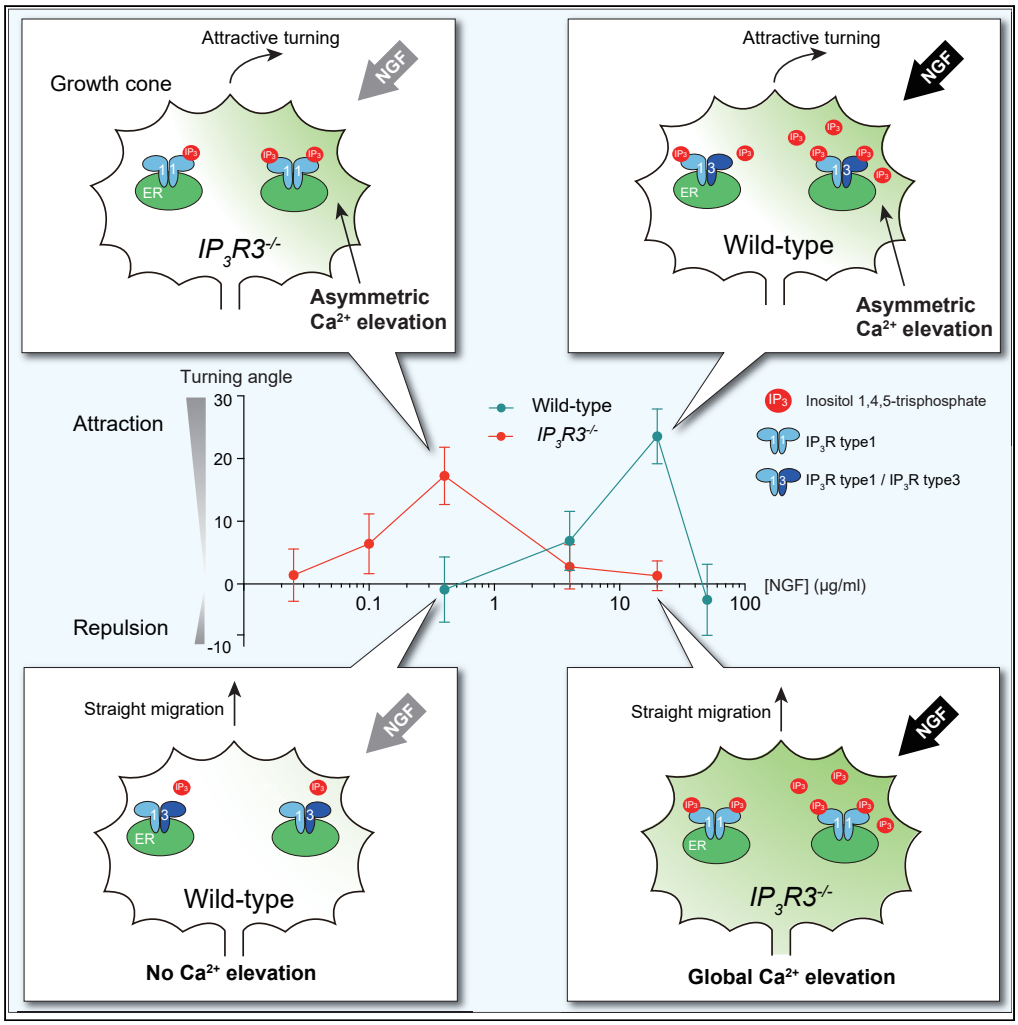

Carmen Chan, Noriko Ooashi, Hiroki Akiyama, ..., Tomomi Shimogori, Katsuhiko Mikoshiba, Hiroyuki Kamiguchi

hiroyuki.kamiguchi@riken.jp

HIGHLIGHTS

IP_3 receptor type 3 (IP_3R3) controls axonal sensitivity to IP_3-based guidance cues

$IP_3R3^{-/-}$ growth cones are not attracted to NGF due to global Ca^{2+} responses

Lower NGF concentrations can polarize $IP_3R3^{-/-}$ growth cones for attractive turning

NGF knockdown *in vivo* can revert abnormal trajectory of $IP_3R3^{-/-}$ axons

Chan et al., iScience *23*, 100963
March 27, 2020
https://doi.org/10.1016/j.isci.2020.100963

iScience

CellPress

Article

Inositol 1,4,5-Trisphosphate Receptor Type 3 Regulates Neuronal Growth Cone Sensitivity to Guidance Signals

Carmen Chan,[1] Noriko Ooashi,[1] Hiroki Akiyama,[2] Tetsuko Fukuda,[1] Mariko Inoue,[1] Toru Matsu-ura,[3] Tomomi Shimogori,[1] Katsuhiko Mikoshiba,[4] and Hiroyuki Kamiguchi[1,5,*]

SUMMARY

During neurodevelopment, the growth cone deciphers directional information from extracellular guidance cues presented as shallow concentration gradients via signal amplification. However, it remains unclear how the growth cone controls this amplification process during its navigation through an environment in which basal cue concentrations vary widely. Here, we identified inositol 1,4,5-trisphosphate (IP_3) receptor type 3 as a regulator of axonal sensitivity to guidance cues *in vitro* and *in vivo*. Growth cones lacking the type 3 subunit are hypersensitive to nerve growth factor (NGF), an IP_3-dependent attractive cue, and incapable of turning toward normal concentration ranges of NGF to which wild-type growth cones respond. This is due to globally, but not asymmetrically, activated Ca^{2+} signaling in the hypersensitive growth cones. Remarkably, lower NGF concentrations can polarize growth cones for turning if IP_3 receptor type 3 is deficient. These data suggest a subtype-specific IP_3 receptor function in sensitivity adjustment during axon navigation.

INTRODUCTION

During neurodevelopment, an axon in search of its appropriate target relies on the navigational activity of its distal end called the growth cone, which senses molecular guidance cues in the immediate environment and makes path-finding decisions at choice points. These guidance cues can be presented as a shallow gradient among a noisy background, with spatial and temporal variations in cue concentrations. Consequently, the growth cone needs to not only amplify guidance signals but also adjust its sensitivity as it migrates through different segments along the chemical gradient. One important challenge for understanding axon guidance is to decipher whether and how intracellular second messengers, critical components mediating signal amplification and growth cone polarization for turning, can also control its sensitivity to guidance signals.

Both attractive and repulsive cues instruct growth cone turning through, in most cases, asymmetric Ca^{2+} elevations with higher Ca^{2+} concentrations on the side of the growth cone facing the source of the cues (reviewed in Gomez and Zheng, 2006). Whether the growth cone turns toward the higher Ca^{2+} side (attraction) or the lower Ca^{2+} side (repulsion) depends, in principle, on the source of Ca^{2+} signals: Ca^{2+} release from the ER triggers attraction, whereas Ca^{2+} influx through plasma membrane channels induces repulsion (reviewed in Tojima et al., 2011). Inositol 1,4,5-trisphosphate (IP_3) is one important second messenger produced from membrane phospholipids and, upon binding to tetrameric IP_3 receptors (IP_3Rs) on the ER, can elicit Ca^{2+} release from the ER into the cytosol (reviewed in Mikoshiba, 2007). This process is commonly termed IP_3-induced Ca^{2+} release (IICR).

In the skin, nerve growth factor (NGF) produced by epidermal keratinocytes (Botchkarev et al., 2006) participates in target field innervation by sensory neurons (Albers et al., 1994; Patel et al., 2000). Also, *in vitro* studies demonstrated that NGF acts as an attractive axon guidance cue through binding to tropomyosin receptor kinase A (TrkA) receptor and activating phospholipase C, an enzyme that catalyzes the hydrolytic conversion of membrane phospholipids into diacylglycerol and IP_3 (Gallo et al., 1997; Ming et al., 1999). Our subsequent work showed that, in a growth cone migrating in an extracellular NGF gradient, phospholipase-C-dependent production of IP_3 and ensuing IICR occurs on the side of the growth cone facing higher NGF concentrations (Akiyama et al., 2009) and that this asymmetric IICR causes polarized membrane dynamics leading to attractive axon turning toward NGF (Akiyama and Kamiguchi, 2010). In

[1]RIKEN Center for Brain Science, 2-1 Hirosawa, Wako City, Saitama 351-0198, Japan

[2]Advanced Research Center for Human Sciences, Waseda University, Tokorozawa, Saitama 359-1192, Japan

[3]Department of Stem Cell Pathology, Kansai Medical University, 2-5-1 Shin-machi, Hirakata, Osaka 573-1010, Japan

[4]Shanghai Institute for Advanced Immunochemical Studies, ShanghaiTech University, 393 Middle Huaxia Road, Shanghai 201210, China

[5]Lead Contact

*Correspondence: hiroyuki.kamiguchi@riken.jp

https://doi.org/10.1016/j.isci.2020.100963

this way, IP_3-induced asymmetric Ca^{2+} signals across the growth cone mediate attractive guidance responses to physiological cues such as NGF.

Although a growth cone can adjust its sensitivity to a wide range of guidance cue concentrations via multiple mechanisms such as receptor internalization and turnover (reviewed in Gallo and Letourneau, 2002; Ming et al., 2002; Piper et al., 2005), a potential role for second messenger signaling in this adjustment process remains to be determined. In the current study, we investigate NGF-dependent axon guidance using mice lacking each of the three IP_3R subunits identified in mammals—type 1 (Furuichi et al., 1989), type 2 (Südhof et al., 1991), and type 3 (Blondel et al., 1993), abbreviated respectively as IP_3R1, IP_3R2, and IP_3R3. These subunits can form a homo- or heterotetrameric IP_3R that acts as a functional Ca^{2+} channel upon IP_3 binding to each subunit (Maes et al., 2001; Monkawa et al., 1995; Nucifora et al., 1996; Wojcikiewicz and He, 1995). Navigational behavior of dorsal root ganglion (DRG) neurons derived from IP_3R1 knockout (R1KO) and IP_3R2 knockout (R2KO) mice are indistinguishable from that of wild-type (WT) neurons. However, DRG neuronal growth cones of IP_3R3 knockout (R3KO) mice cannot respond properly to normal concentration ranges of NGF *in vitro* and in the skin *in vivo*, most likely because they are hypersensitive to IP_3 and therefore exhibit global Ca^{2+} elevations in response to NGF gradients. These data raise the possibility that growth cones could adjust their sensitivity at the IP_3R level such that they continue to produce polarized signals even in the presence of local variations in guidance cue concentrations.

RESULTS

Subtype-Specific IP_3R Involvement in Growth Cone Turning Responses

Although it is known that asymmetric IICR across the growth cone plays a crucial role in axon guidance mediated by extracellular cues such as NGF, which one(s) of the three mammalian IP_3R subtypes participates in this process remains unclear. We employed focal laser-induced photolysis (FLIP) of caged IP_3 to generate spatially localized IP_3 signals in growth cones derived from IP_3R-subtype-specific knockout mice. For loading, DRG neurons were incubated with 0.5 μM solution of caged IP_3. In our previous study using chicken neurons (Akiyama et al., 2009), FLIP of caged IP_3 resulted in a sustained increase in IP_3 and its consequent Ca^{2+} elevation on the side of the growth cone receiving laser irradiation ("near side"). These asymmetric signals caused growth cone attractive turning toward higher IP_3 and Ca^{2+}.

In the current experiments, DRG growth cones from WT mice also turned attractively toward higher IP_3, whereas control growth cones that had not been loaded with caged IP_3 showed no detectable turning after laser irradiation (Figures 1A and 1B). As the occurrence of IICR depends on cytosolic levels of cyclic adenosine monophosphate (cAMP), chicken neurons cultured on a laminin substrate in our previous study, which caused a reduction in cAMP levels in growth cones, failed to respond to IP_3 signals (Akiyama et al., 2009). Consistently, IP_3-induced turning of mouse neuronal growth cones was also dependent on cAMP because the cAMP antagonist Rp-cAMPS (20 μM) blocked the effect of IP_3 uncaging (Figure 1B). Analyses of neurons derived from IP_3R-subtype-specific knockout mice showed that R1KO or R2KO growth cones turned toward higher IP_3 (Figure 1B). By contrast, R3KO growth cones showed no significant turning (Figures 1A and 1B), indicating that IP_3R3 is necessary for turning responses to IP_3 under this experimental condition.

We next tested whether an extracellular NGF gradient was attractive to DRG growth cones from WT and each of the three knockout mice. In these assays, NGF concentrations near the growth cones were approximately 0.1% of in-pipette concentration of 20 μg/mL (Lohof et al., 1992). The NGF gradient attracted WT, R1KO and R2KO growth cones, but not R3KO growth cones (Figures 1C and 1D). The migration speed of growth cones in NGF gradients was not affected by the loss of each IP_3R subtype (Figure S1). Because attractive turning responses of WT and R1KO growth cones may potentially be different quantitatively, we calculated Cohen's d between WT and R1KO to be 0.23 for IP_3 uncaging (Figure 1B) and 0.69 for NGF gradients (Figure 1D), suggesting that the effect of R1KO is small to moderate. Nonetheless, we concluded that, at least qualitatively, R1KO growth cones are indistinguishable from WT growth cones in their responses to IP_3 and NGF signals. As a control to show that R3KO growth cones were still able to turn, we examined the effect of myelin-associated glycoprotein (MAG) known to attract nascent axons via Ca^{2+} release from the ER through another class of Ca^{2+} channels, ryanodine receptors (Henley et al., 2004; Tojima et al., 2014). Consistent with such differences in the requirement of ion channels mediating Ca^{2+} release, MAG caused attractive turning of R3KO growth cones (Figure 1E). Therefore, the loss of IP_3R3 rendered growth cones unresponsive to an IP_3R-based guidance cue such as NGF.

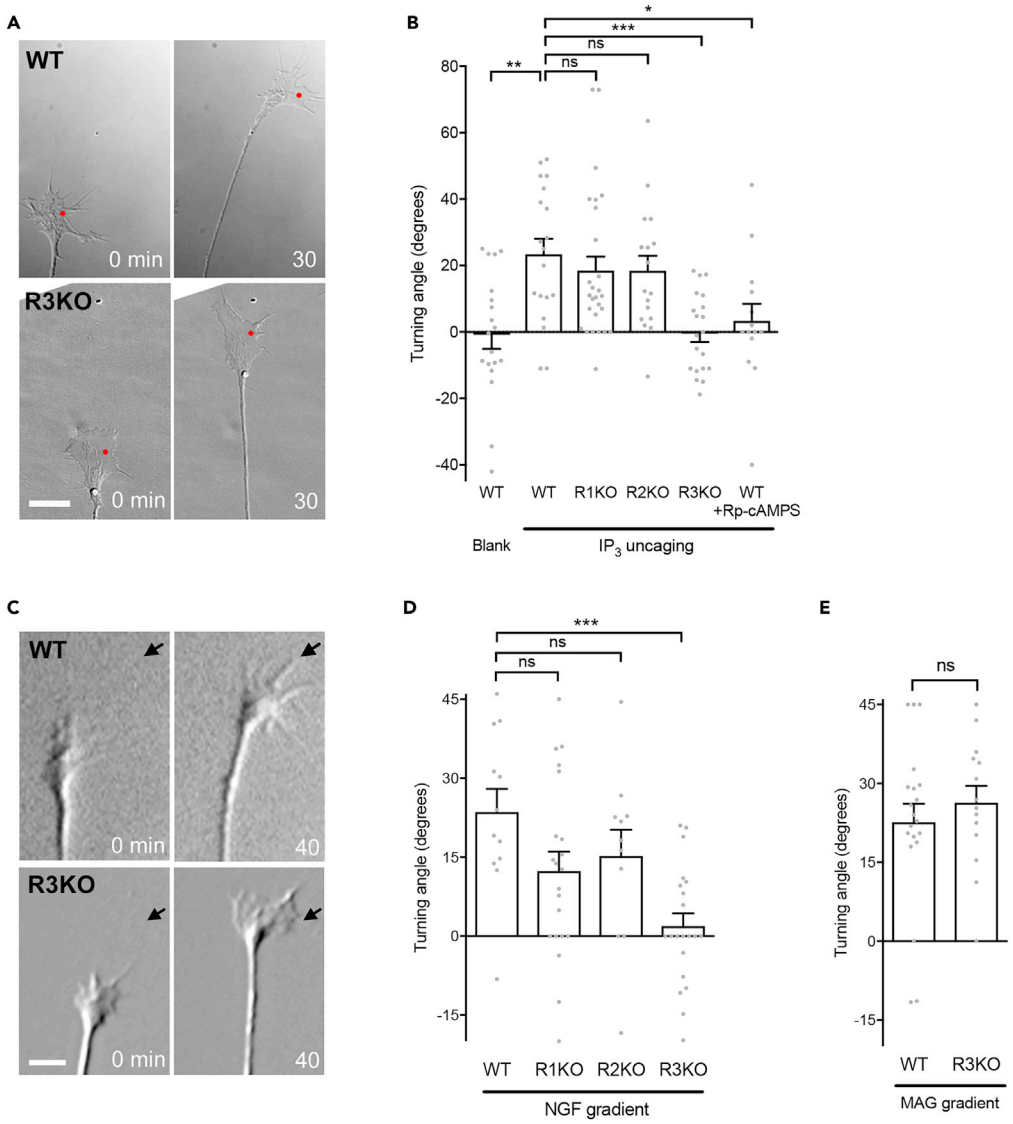

Figure 1. Subtype-Specific IP_3R Involvement in Growth Cone Turning Responses

(A) Caged IP_3 was photolyzed at the red spots to generate spatially localized IP_3 elevations. Shown are representative growth cones of WT (upper panels) and R3KO (lower panels) neurons at the beginning (0 min) and end (30 min) of repetitive FLIP. Scale bar, 10 μm.

(B) Mean turning angles of WT and IP_3R subtype-specific knockout growth cones 30 min after the onset of repetitive FLIP, with or without ("Blank") preloading of caged IP_3. The rightmost bar indicates data from WT growth cones in the presence of bath-applied Rp-cAMPS (20 μM). Positive angles represent attractive turning toward the side with laser irradiation. Bars represent mean ± SEM, with each gray dot indicating turning angle of individual growth cones in this experiment. *$p < 0.05$; **$p < 0.01$; ***$p < 0.001$; ns, not significant; Dunnett's test.

(C) WT and R3KO growth cones immediately before and 40 min after the onset of repetitive NGF ejection from the direction indicated by the arrows. Scale bar, 10 μm.

(D and E) Average turning angles of WT and IP_3R subtype-specific knockout growth cones 40 min after the start of repetitive ejection of NGF (D) or MAG (E). Bars represent mean ± SEM, with each gray dot indicating turning angle of individual growth cones in this experiment. ***$p < 0.001$; ns, not significant; Dunnett's test (D) or Student's *t* test (E). See also Figure S1.

Although IP_3R1 and IP_3R3 are expressed by neurons, IP_3R2 is detectable only in glial cells in the nervous system (Sharp et al., 1999; Taylor et al., 1999). Consistent with this glial-specific expression pattern of IP_3R2, our results showed that IP_3R2 was dispensable for IP_3-dependent growth cone turning. Therefore, we decided to leave out R2KO mice in subsequent experiments.

Growth Cone Turning Responses Correlate with Ca^{2+} Signal Asymmetry

To investigate a correlation between growth cone turning and intracellular signaling asymmetry, we monitored spatiotemporal dynamics of Ca^{2+} in response to localized IP_3 signals. In WT and R1KO growth cones, IP_3 uncaging resulted in Ca^{2+} elevations on the near side but no detectable Ca^{2+} increases on the opposite "far" side (Figures 2A–2C). Such asymmetric Ca^{2+} signals are consistent with the ability of these growth cones to turn toward the side with IP_3 production. By contrast, R3KO growth cones showed widespread increases in Ca^{2+} spanning both the near and far sides after localized IP_3 uncaging on the near side (Figures 2A–2C). To capture a potential timepoint when Ca^{2+} gradients could be formed in R3KO growth cones, we compared Ca^{2+} levels between the near and far sides during earlier periods after IP_3uncaging. As shown in Figure 2D, localized IP_3 production caused a transient asymmetry in Ca^{2+} concentrations across the R3KO growth cone at 30–60 s but could not sustain the Ca^{2+} gradient after 1 min of the onset of IP_3 uncaging (Figures 2C and 2D), suggesting that R3KO growth cones have symmetric IICR on the timescale for axon turning processes. We also tested whether extracellular NGF gradients cause similar spatiotemporal dynamics of Ca^{2+} in growth cones, using ratiometric Oregon Green 488 BAPTA-1 (OGB-1)–Fura-red (FR) imaging as a measure of Ca^{2+} levels. NGF gradients induced Ca^{2+} elevations only on the near side of WT and R1KO growth cones but caused widespread Ca^{2+} increases on both sides of R3KO growth cones (Figure 3). These results suggest that the failure of R3KO growth cones to turn toward NGF-induced IP_3 signals may be due to symmetric Ca^{2+} elevations, a distribution pattern that is unlikely to act as a polarizing signal.

One possible explanation for the lack of Ca^{2+} signal asymmetry in R3KO growth cones is widespread distribution of IP_3 due to faster diffusion or slower degradation of IP_3. To test for this possibility, we monitored spatiotemporal dynamics of IP_3 that had been photo-released from caged IP_3, using the IP_3 sensor IRIS-2.3 (Matsu-ura et al., 2019). This sensor contains enhanced green fluorescent protein (EGFP) and HaloTag- tetramethylrhodamine (TMR), and the efficiency of fluorescence resonance energy transfer (FRET) from EGFP to TMR decreases upon IP_3 binding to IRIS-2.3. Therefore, we calculated the inverse FRET ratio in IRIS-2.3, i.e., the ratio of EGFP emission compared with TMR emission (F_{EGFP}/F_{TMR}) as a measure of IP_3 levels. In both WT and R3KO neurons, IP_3uncaging on one side of the growth cone resulted in asymmetric increases in IP_3, with IP_3 levels on the near side being significantly higher than those on the far side (Figures 4A–4C). Similarly, NGF gradients induced IP_3 elevations only on the near sides of both WT and R3KO growth cones (Figures 4D–4F). These data indicate that spatiotemporal dynamics of IP_3 is indistinguishable between WT and R3KO growth cones and that the lack of Ca^{2+} signal asymmetry in R3KO growth cones is not attributable to altered IP_3 dynamics.

Another possible explanation for the lack of Ca^{2+} signal asymmetry in R3KO growth cones is increased expression of NGF downstream signaling components such as TrkA and IP_3R1, in which the far side of R3KO growth cones could respond to lower concentrations of NGF. However, these possibilities are unlikely because we could not detect any substantial increase in the amount of TrkA and IP_3R1 expressed in DRGs of R3KO mice (Figure S2).

R3KO Growth Cones Are Hypersensitive to IP_3-Based Guidance Signals

In R3KO growth cones, symmetric Ca^{2+} elevations in spite of asymmetric IP_3 signals suggest the presence of hypersensitive IP_3Rs that can be maximally activated by physiological IP_3 signals, such as those in the growth cone near side, and also generate substantial Ca^{2+} release in response to low levels of IP_3, such as those in the growth cone far side. To test for this hypothesis, we monitored Ca^{2+} responses to low-amplitude IP_3 signals generated by FLIP of a smaller amount of caged IP_3, i.e., 0.1 μM in contrast to 0.5 μM in previous experiments (Figures 1A, 1B, and 2). These low-amplitude IP_3 signals attracted R3KO growth cones but had no detectable effect on directional preference of WT growth cones (Figure 5A). Consistent with these turning responses, R3KO growth cones exhibited asymmetric Ca^{2+} elevations with higher Ca^{2+} on the side with IP_3 uncaging, whereas WT growth cones showed no detectable Ca^{2+} increases presumably because the amplitude of IP_3 signals were below the threshold for IICR (Figures 5B and 5C).

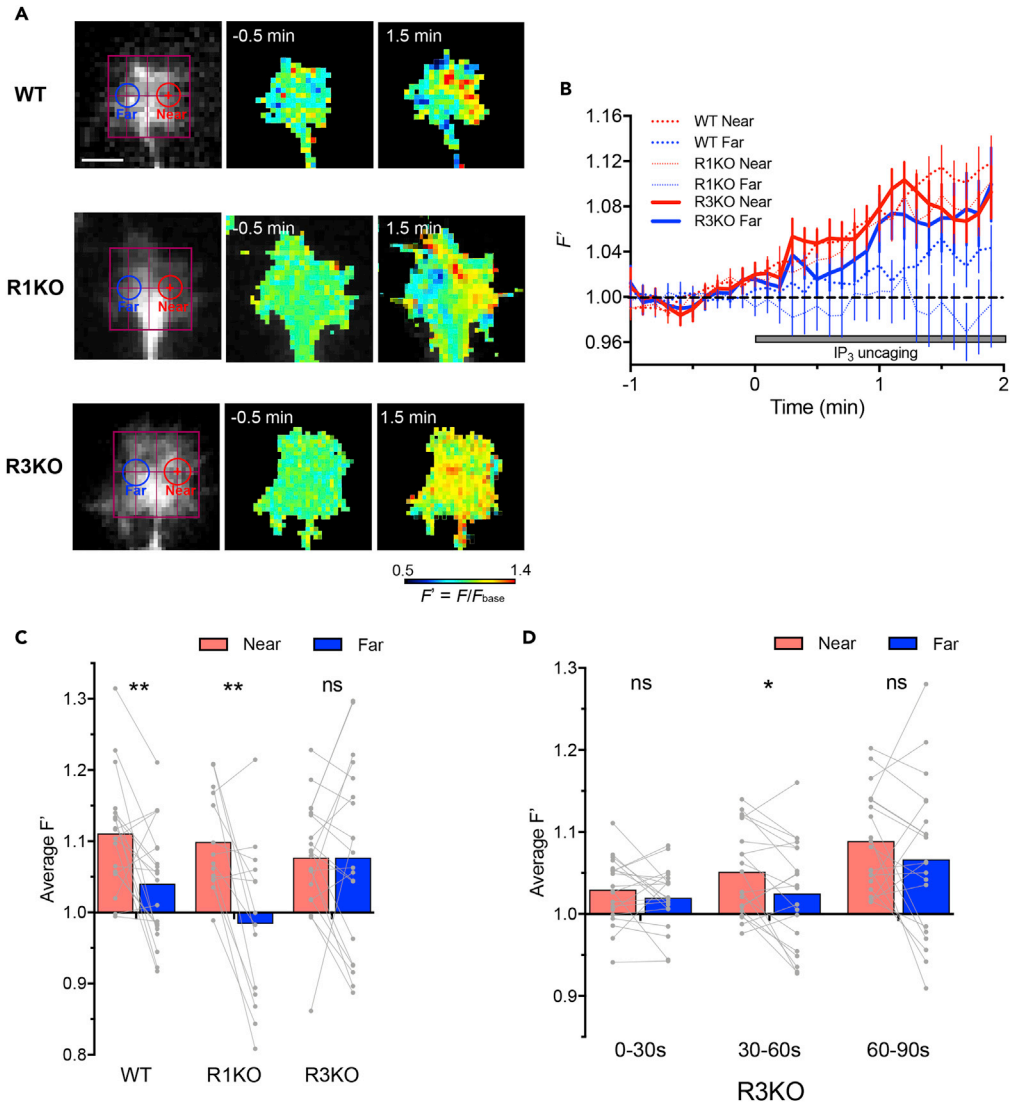

Figure 2. Spatiotemporal Dynamics of Ca^{2+} in Growth Cones Responding to Localized IP_3 Signals

(A) Pseudo-color Ca^{2+} images in WT, R1KO, and R3KO growth cones 0.5 min before and 1.5 min after the onset of repetitive FLIP of caged IP_3. The red crosshairs represent the sites of laser irradiation. Relative changes in Fluo-8H fluorescence (F/F_{base}, defined as F') were used as a measure of cytosolic Ca^{2+} levels. The near side ROI (red) was defined as a circular region whose center corresponded to the site of laser irradiation and whose diameter equaled to one-third of the width of each growth cone. The far side ROI (blue) was defined as a circular region of the same diameter that was placed on the center of the far-side half of each growth cone. Scale bar, 5 μm.

(B) Time course changes in F' in the near (red line) and far (blue line) ROIs positioned on WT (dotted line), R1KO (finely dotted line), and R3KO (solid line) growth cones. Data are represented as mean ± SEM.

(C and D) The mean amplitude of F' during 90–120 s (C) and earlier periods (D) after the onset of repetitive FLIP shown in (B). Data on WT, R1KO, and R3KO neurons were included in (C), and data on only R3KO neurons in (D). Each gray line connecting two dots represents data from the near and far ROIs of a single growth cone, and each colored bar represents the mean. *$p < 0.05$; **$p < 0.01$; ns, not significant; paired *t* test.

See also Figure S2.

We also examined the effect of lower-concentration NGF gradients, i.e., 0.4 μg/mL NGF in pipette in contrast to 20 μg/mL in previous experiments (Figures 1C, 1D, and 3). These NGF gradients induced neither Ca^{2+} elevations nor turning responses in WT growth cones but caused asymmetric Ca^{2+} signals and attractive turning responses in R3KO growth cones (Figures 5D–5F). These data support our notion that R3KO growth cones are hypersensitive to IP_3-based guidance cues such as NGF.

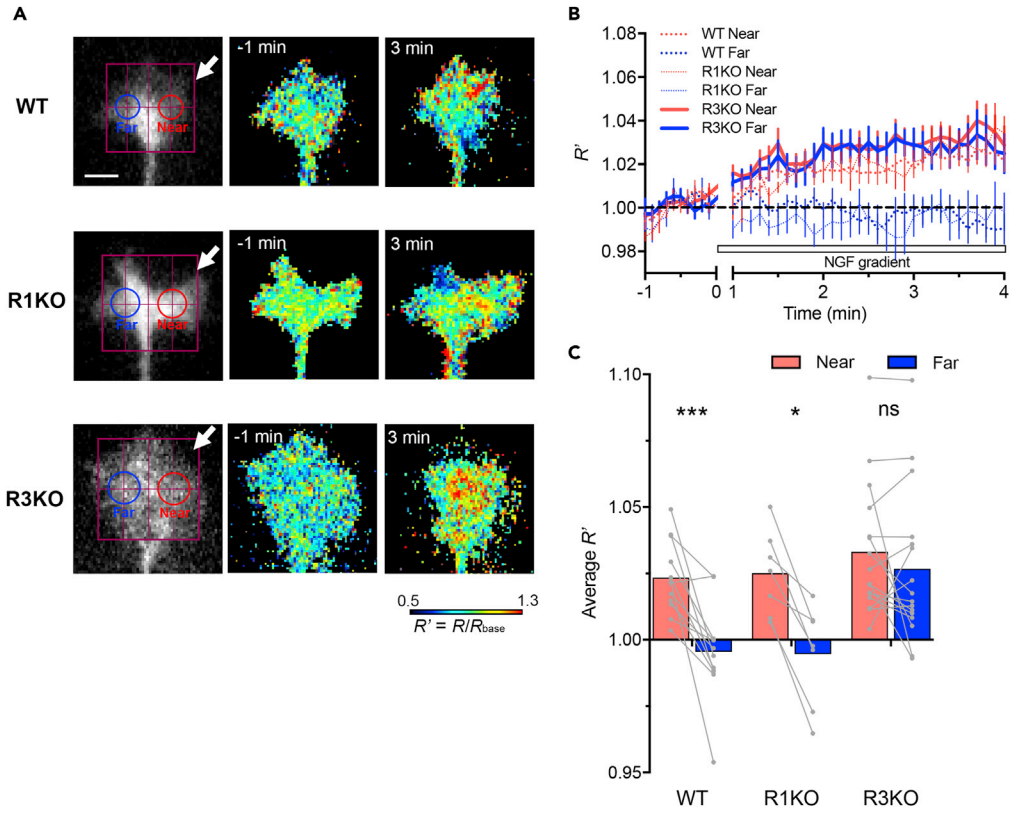

Figure 3. Spatiotemporal Dynamics of Ca^{2+} in Growth Cones Responding to NGF Gradients

(A) Pseudo-color Ca^{2+} images in WT, R1KO, and R3KO growth cones 1 min before and 3.5 min after the onset of repetitive NGF ejection from the direction indicated by the white arrows. The growth cones were preloaded with a ratiometric pair of calcium indicators, OGB-1 and FR, and the OGB-1/FR emission ratio ($F_{OGB\text{-}1}/F_{FR}$, defined as R) was determined. Shown are relative changes in R (R/R_{base}, defined as R') used as a measure of cytosolic Ca^{2+} levels. The near (red) and far (blue) ROIs were defined as described in Figure 2. Scale bar, 5 μm.

(B) Time course changes in R' in the near (red line) and far (blue line) ROIs positioned on WT (dotted line), R1KO (finely dotted line), and R3KO (solid line) growth cones. Data from the first minute after the start of NGF ejection were excluded because of a lack of stable NGF gradients. Data are represented as mean ± SEM.

(C) The mean amplitude of R' over the last 1 min of repetitive NGF ejection shown in (B). Each gray line connecting two dots represents data from the near and far ROIs of a single growth cone, and each colored bar represents the mean. *$p < 0.05$; ***$p < 0.001$; ns, not significant; Wilcoxon matched pairs signed rank test.

See also Figure S2.

To determine growth cone sensitivity more comprehensively, we analyzed the effect of other NGF concentrations on axon turning responses using WT- and IP_3R-subtype-specific knockout neurons. Dose-response curves were generated by plotting axon turning angles against log-scale NGF concentrations in micropipette (Figure 6). WT and R1KO growth cones were responsive to similar concentration ranges of NGF, but the curve for R3KO growth cones shifted to lower concentration ranges of NGF. Collectively, our results suggest that growth cones can respond to different concentration ranges of IP_3-based guidance cues depending on whether IP_3R3 participates in the generation of IICR.

If R3KO axons are hypersensitive, partial inhibition of a remaining IP_3R subtype in these axons, IP_3R1, should restore their sensitivity to NGF into normal ranges. It is known that cAMP-dependent phosphorylation of IP_3R1 is necessary for IICR (Nakade et al., 1994) and that the cAMP antagonist Rp-cAMPS blocks axonal responses to IP_3-mediated guidance signals such as NGF (Akiyama et al., 2009). Therefore, instead of a commonly used Rp-cAMPS concentration of 20 μM, we treated R3KO neurons with 0.4 μM Rp-cAMPS that corresponded to 5% of a reported Ki of 8 μM (Van Haastert et al., 1984). Such mild treatment caused R3KO axons to recover attractive turning responses to a normal concentration range of NGF (20 μg/mL in pipette): turning angle (mean ± SEM) = 1.7° ± 3.0° (19 untreated axons) versus

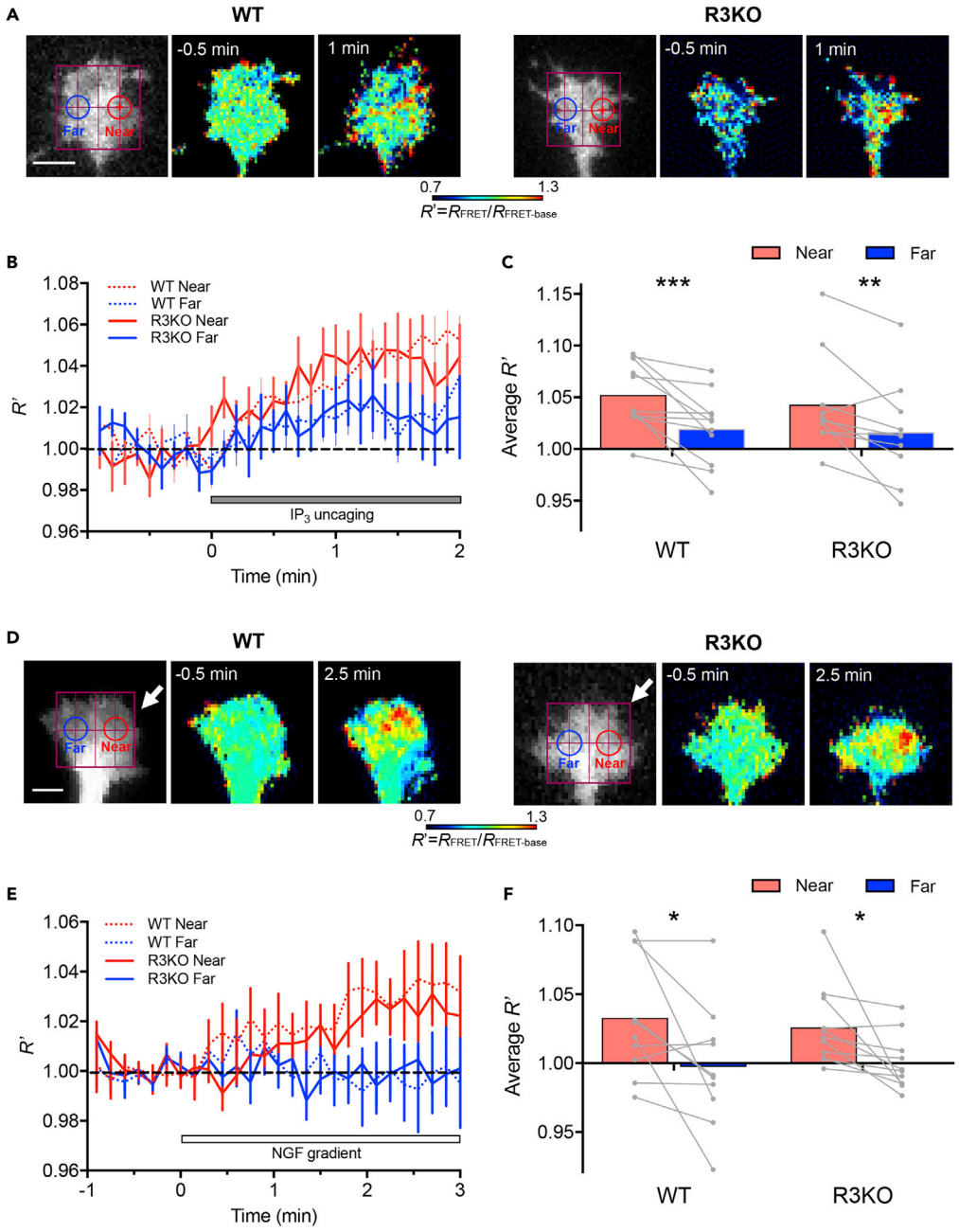

Figure 4. Spatiotemporal Dynamics of IP_3 in Growth Cones Responding to Localized IP_3 Signals or NGF Gradients

(A) Pseudo-color IP_3 images in WT and R3KO growth cones 0.5 min before and 1 min after the onset of repetitive FLIP of caged IP_3. Each growth cone was transfected with the FRET-based IP_3 sensor IRIS-2.3 containing EGFP and HaloTag-TMR, and the ratio of EGFP emission compared with TMR emission (F_{EGFP}/F_{TMR}, defined as R_{FRET}) was determined. Shown are relative changes in R_{FRET} ($R_{FRET}/R_{FRET\text{-}base}$, defined as R') used as a measure of IP_3 levels. The red crosshair indicates the site of laser irradiation. The near (red) and far (blue) ROIs were defined as described in Figure 2. Scale bar, 5 μm.

(B) Time course changes in R' in the near (red line) and far (blue line) ROIs positioned on WT (dotted line) and R3KO (solid line) growth cones.

(C) The mean amplitude of R' over the last 30 s of repetitive FLIP shown in (B). **p < 0.01; ***p < 0.001, Wilcoxon matched pairs signed rank test.

(D) Pseudo-color IP_3 images in WT and R3KO growth cones 0.5 min before and 2.5 min after the onset of repetitive NGF ejection from the direction indicated by the white arrows. Scale bar, 5 μm.

Figure 4. *Continued*

(E) Time course changes in *R*′ in the near (red line) and far (blue line) ROIs positioned on WT (dotted line) and R3KO (solid line) growth cones.

(F) The mean amplitude of *R*′ over the last 1 min of repetitive NGF ejection. *$p < 0.05$; paired *t* test.

In (B and E), data are represented as mean ± SEM. In (C and F), each gray line connecting two dots represents data from the near and far ROIs of a single growth cone, and each colored bar represents the mean.

10.5° ± 2.7° (19 Rp-cAMPS-treated axons), $p < 0.05$; student's *t* test. These data further support our notion that IP_3R sensitivity, which can be regulated by cAMP-dependent phosphorylation, is an important determinant of optimal concentration ranges of NGF for axon guidance.

NGF Downregulation Restores R3KO Axon Trajectory in the Skin

To validate *in vivo* physiological significance of our findings, we compared projection patterns of NGF-responsive TrkA-expressing sensory axons in the hindpaw skin of WT versus R3KO mice. Sensory axons in the hindpaw skin is one of the most well-studied models, and axon projection patterns are relatively easy to quantify (Patel et al., 2000; Wang et al., 2013). We analyzed four pairs of WT/R3KO littermates from IP_3R3 heterozygous-heterozygous mating. The border between epidermis and dermis was evident because the epidermis except for its basal layer, but not the dermis, is immunopositive for NGF (Botchkarev et al., 2006). We observed that TrkA-positive axons in the epidermis of WT and R3KO mice had different morphologies: WT axons were straighter and well organized (relatively evenly spaced), whereas R3KO axons were undulating and appeared to follow meandering paths (Figure 7A). Such abnormal trajectories of R3KO axons in the skin were also observed in cleared whole-mount tissues where TrkA-positive axons were three-dimensionally reconstructed (Videos S1 and S2). To quantify axon morphological characteristics on skin sections, we employed a "curviness index" of each TrkA-positive axon in the NGF-positive epidermis (see Transparent Methods). The curviness index of 1 indicates the completely straight axon trajectory, whereas larger values represent more curly axons. As shown in Figures 7B and 7C, R3KO axons had significantly larger curviness index than WT axons, confirming our observation that R3KO axons have abnormal trajectories in the skin.

To test whether the observed abnormality of R3KO axons in the skin is due to their intrinsic characteristics, we cultured dissociated WT and R3KO DRG neurons *in vitro* and compared their axon morphologies. We confirmed that the lack of IP_3R3 did not cause any innate growth defects or curliness in DRG axons (Figure S3), excluding the possibility that the undulated morphology of R3KO axons *in vivo* is due to any intrinsic defects in directional growth. Furthermore, because skin keratinocytes from WT and R3KO mice release comparable amounts of NGF (Figure S4A), it is unlikely that a drastic alteration in the level of epidermal NGF in R3KO mice causes TrkA axons to meander in the skin.

If the curly phenotype of R3KO axons is due to their hypersensitivity that renders growth cones irresponsive to epidermal NGF, then this phenotype should be reverted back to normal trajectory when epidermal NGF levels are lowered. To control NGF expression in the epidermis, we obtained short hairpin RNA (shRNA) against NGF and confirmed its knocking down effect using cultured primary keratinocytes (Figure S4B). We then analyzed the morphology of TrkA axons in the epidermal area transfected with either NGF shRNA or control shRNA plasmid (Figures 8A–8C). The curviness index of R3KO axons was shifted toward 1 in the epidermal area transfected with NGF shRNA, but not with control shRNA (Figure 8D), indicating that NGF downregulation can antagonize the effect of IP_3R3 deficiency on the trajectory of TrkA axons. By contrast, NGF downregulation did not significantly affect the trajectory of TrkA axons in WT mice (Figure 8D). These findings are consistent with our model that the lack of IP_3R3 subunit causes DRG sensory axons to be hypersensitive to NGF and therefore unable to extend properly into the epidermis.

DISCUSSION

We identified the IP_3R3 subunit as a regulator of growth cone sensitivity to guidance signals *in vitro* and *in vivo* and demonstrated the correlation between IICR asymmetry and turning competency when encountering various concentration ranges of the IP_3-based guidance cue NGF. Compared with WT growth cones that respond to "normal" concentrations of NGF, IP_3R3 deficiency renders growth cones hypersensitive, in which the growth cones are either able to detect lower than "normal" concentrations of NGF or unable to respond to "normal" concentrations of NGF because intracellular second messenger

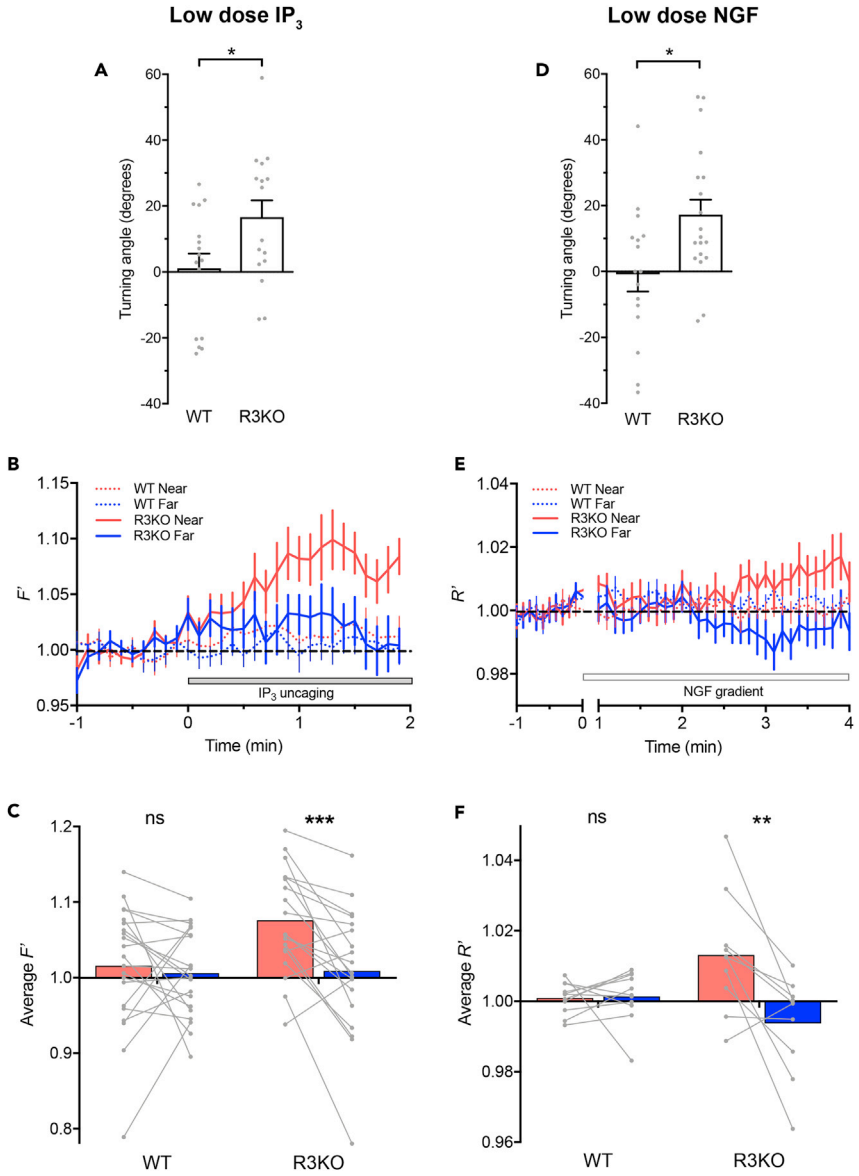

Figure 5. R3KO Growth Cones Are Hypersensitive to IP_3-Based Guidance Signals

Shown are growth cone responses to lower doses of IP_3 (A–C) and NGF (D–F).

(A) Average turning angles of WT and R3KO growth cones 30 min after the onset of repetitive FLIP of a smaller amount of caged IP_3 (0.1 μM in contrast to 0.5 μM in Figure 1B). *$p < 0.05$; student's *t* test.

(B) Time course changes in *F′*, calculated as F/F_{base} of Fluo-8H fluorescence, in the near (red line) and far (blue line) ROIs positioned on WT (dotted line) and R3KO (solid line) growth cones in response to repetitive FLIP of a smaller amount of caged IP_3 (0.1 μM in contrast to 0.5 μM in Figure 2B).

(C) The mean amplitude of *F′* over the last 30 s of repetitive FLIP shown in (B). ***$p < 0.001$; ns, not significant; paired *t* test.

(D) Average turning angles of WT and R3KO growth cones 40 min after the start of repetitive ejection of NGF. In-pipette concentration of NGF was 0.4 μg/mL in contrast to 20 μg/mL in Figure 1D. *$p < 0.05$; student's *t* test.

(E) Time course changes in *R′*, calculated as R/R_{base} of a ratiometric pair of OGB-1 and FR, in the near (red line) and far (blue line) ROIs positioned on WT (dotted line) and R3KO (solid line) growth cones in response to NGF gradients. In-pipette concentration of NGF was 0.4 μg/mL NGF in contrast to 20 μg/mL in Figure 3B.

(F) The mean amplitude of *R′* over the last 1 min of repetitive NGF ejection shown in (E). **$p < 0.01$; ns, not significant; Wilcoxon matched pairs signed rank test. In (A and D), bars represent mean ± SEM, with each gray dot indicating turning angle of individual growth cones in this experiment.

In (B and E), data are represented as mean ± SEM. In (C and F), each gray line connecting two dots represents data from the near and far ROIs of a single growth cone, and each colored bar represents the mean.

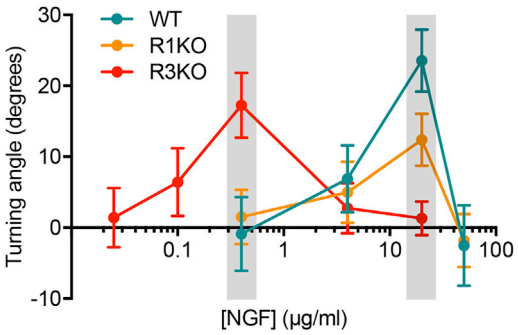

Figure 6. Optimal Concentration Ranges of NGF for Growth Cone Attractive Responses

Turning angles of WT, R1KO, and R3KO growth cones were determined 40 min after the start of repetitive ejection of various concentrations of NGF. Dose-response curves were generated by plotting the average angles against the log-scale of NGF concentration in the pipette. Data points in gray boxes are the same as those presented in Figures 1D and 5D. The number of growth cones assayed for each concentration was 11–22. Data are represented as mean ± SEM.

signaling is saturated and symmetric across the growth cone axis. Our FLIP experiments using different concentrations of caged IP_3 showed that IP_3R3-dependent adjustment of growth cone sensitivity occurs at the level of IP_3 detection, suggesting that functional tetrameric IP_3Rs composed without the type 3 subunit are hypersensitive and can mediate IICR in response to low levels of IP_3.

One prominent difference among the three IP_3R subtypes is their affinities for IP_3. IP_3R3 is known to have lower affinity compared with IP_3R1 and IP_3R2 (Iwai et al., 2005; Newton et al., 1994; Wojcikiewicz and Luo, 1998). Because IP_3 affinity of each IP_3R subtype is tightly correlated with its IP_3 sensitivity (Wojcikiewicz and Luo, 1998), the three subtypes can be activated to different extent within certain ranges of IP_3 concentrations in the cytosol. In other words, IP_3R3 should be least sensitive to increases in cytosolic IP_3 concentrations and requires relatively high levels of IP_3 for its activation. WT neurons express IP_3R1 and IP_3R3 but not IP_3R2, and it has been shown that IP_3R1 and IP_3R3 can form a heterotetrameric IP_3R (Miyakawa et al., 1999). Based on our data and previous findings, we propose a model of how IP_3R3 controls growth cone sensitivity to guidance signals (Figure S5). In WT growth cones, a homo- or heterotetrameric IP_3R comprising IP_3R3 may be activated only where there is a substantial amount of IP_3 such as the growth cone near side. By contrast, in R3KO growth cones that also lack the expression of glial IP_3R2, a homotetrameric IP_3R composed solely of the high-affinity IP_3R1 can mediate substantial IICR even where there is a small amount of IP_3 such as the growth cone far side (Figure S5).

Other mechanisms have been suggested as to how growth cones can adjust their sensitivities to guidance cues, e.g., endocytosis-dependent desensitization and protein-synthesis-dependent resensitization (Ming et al., 2002; Piper et al., 2005). These mechanisms are broadly referred to as growth cone adaptation. One group of researchers, however, has proposed an alternative but not exclusive mechanism that relies on the growth cone's preexisting architecture: through spatiotemporal averaging of guidance cue-receptor binding along the growth cone circumference (Rosoff et al., 2004; Xu et al., 2005). This group used both *in vitro* NGF-elicited DRG axon turning and computer modeling to show that adaptation was not necessary to explain the long-term growth cone responses to gradients of guidance cues. Due to the stochastic nature of ligand-receptor binding, when NGF-receptor binding signals were pooled spatially over the growth cone circumference, and also pooled temporally, growth cones were in theory able to sense the difference in NGF concentration even in shallow gradients and respond correctly by turning.

Although we demonstrated that growth cone sensitivity can be controlled by intracellular signaling at the IP_3R level, it remains unclear how this regulation occurs under physiological conditions. One possible mechanism is phosphorylation of IP_3R subunits (reviewed in Mikoshiba, 2007; Shah et al., 2015; Vanderheyden et al., 2009). For example, cAMP-dependent protein kinase A (PKA) phosphorylates IP_3R3 at three known sites: serines 916, 934, and 1832, in contrast to only one for each of IP_3R1 or IP_3R2. Interestingly, PKA phosphorylation of IP_3R3 can result in enhanced (Chaloux et al., 2007; Dyer et al., 2003; Wojcikiewicz and Luo, 1998) or decreased (Giovannucci et al., 2000; Straub et al., 2002) sensitivity to IP_3, depending on cell type. In DT40 cells, PKA activation results in decreased IICR, but this regulation is not dependent on the three PKA phosphorylation sites on IP_3R3 (Soulsby and Wojcikiewicz, 2007). These findings are consistent with the hypothesis that intracellular signaling components such as PKA regulate IP_3R3 activity via multiple mechanisms and that these mechanisms may control the overall activity of tetrameric IP_3Rs given the particular importance of IP_3R3 for sensitivity regulation.

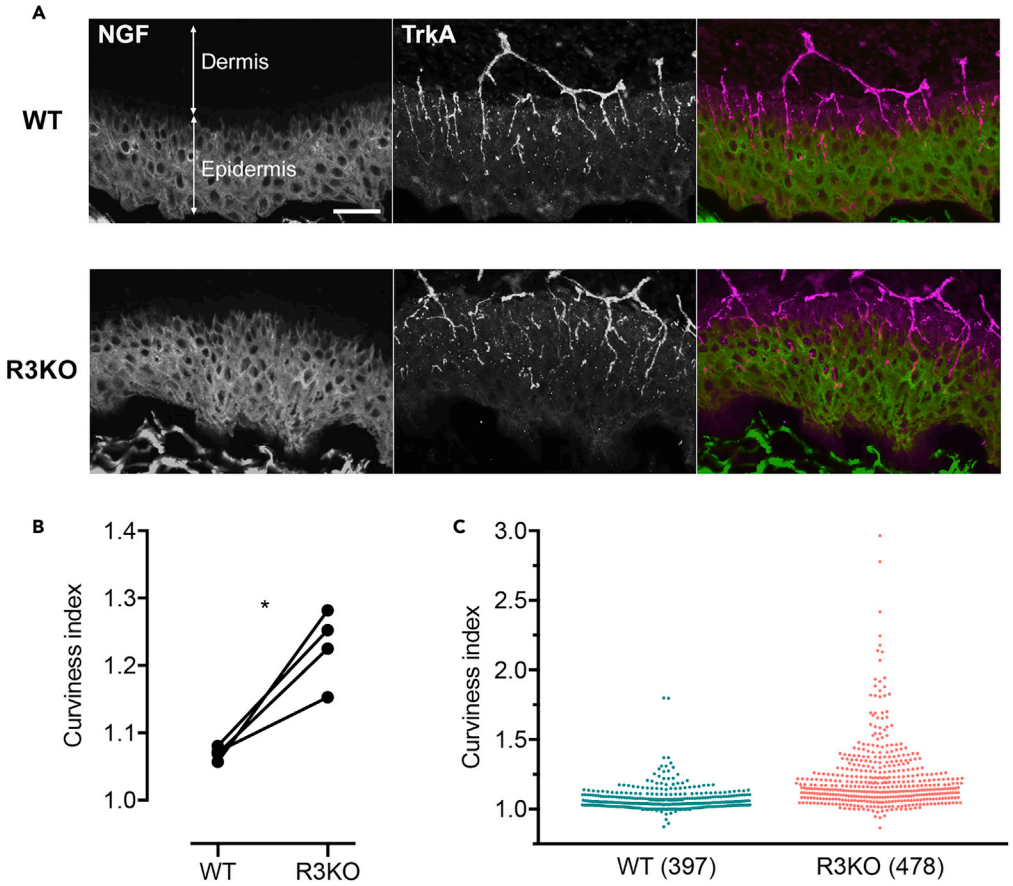

Figure 7. Trajectory of TrkA-Positive Axons in the Skin Epidermis

(A) Sagittal tissue sections of the hindpaw plantar surface from WT and R3KO animals. The sections were immunostained for NGF and TrkA. The superimposed images show NGF in green and TrkA in magenta. Scale bar, 50 μm.

(B) Trajectory of TrkA-positive axons was represented as "curviness index"—the length of each entire axon segment within the NGF-positive area divided by the straight-line distance between the two ends of that segment. Four pairs of WT and R3KO littermates were analyzed. The indexes of TrkA axons were averaged in each animal and compared between R3KO and its WT littermate. *$p < 0.05$; paired *t* test.

(C) The curviness indexes of all axons from the four pairs of animals analyzed in (B) were pooled and presented as scatterplots. Each dot corresponds to a single axon segment (n = 397 for WT, n = 478 for R3KO).

See also Figures S3 and S4.

In the skin, NGF is expressed and secreted by epidermal keratinocytes (Botchkarev et al., 2006). Although not as clear as *in vitro*, NGF may serve axon guidance functions *in vivo*. Rather than acting as a long-range guidance cue, NGF is mainly responsible for the final stages of axon path-finding and target innervation because cutaneous innervation in the hindlimb is lost in the absence of NGF-TrkA signaling (Patel et al., 2000). Moreover, NGF can direct axon growth in transplants after injury to central and peripheral nervous systems (Hu et al., 2010; Ziemba et al., 2008). In *ex utero* slice cultures of mouse embryos, ectopic NGF is able to attract spinal nerve growth to abnormal regions (Tucker et al., 2001). These findings suggest that growing axons *in vivo* can use NGF as a positional cue to reach specific regions or cells, such as TrkA axons extending into the epidermis where keratinocytes secrete NGF.

Our *in vivo* data indicated that the presence of specific IP_3R subtype is important for the formation of normal axon trajectory during skin development. It is well documented that defective guidance during development, e.g., via eliminating the expression of particular guidance cues, causes the axons to display wavy, meandering, and disorderly paths of growth compared with the highly organized and well-defined paths of normal growth (Bentley and Toroian-Raymond, 1986; Enriquez-Barreto et al., 2012; Honig et al., 2002). In our data, R3KO mice had curly sensory axons in the skin epidermis compared with the

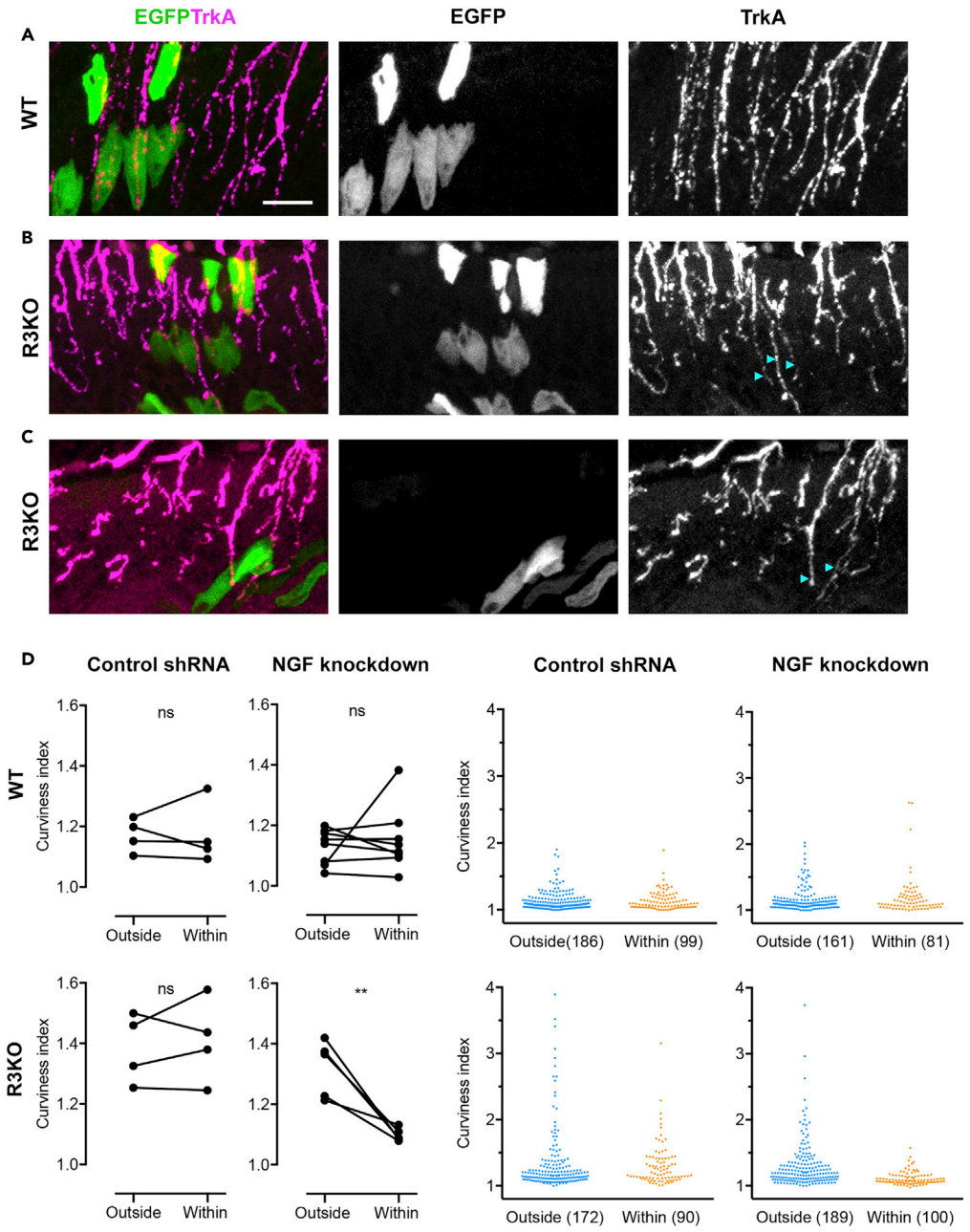

Figure 8. NGF Downregulation Restores R3KO Axon Trajectory in the Skin

(A) Example of Wthindpaw epidermis transfected with control shRNA plasmid. (Left) Superimposition of EGFP (green) and TrkA (magenta). (Middle) EGFP-positive areas representing successful transfection and long-term integration of the shRNA sequence into the genome of skin epidermal cells (mostly keratinocytes). (Right) Immunofluorescence of TrkA axons in the epidermis. Scale bar, 20 μm.

(B and C) Two examples of R3KO hindpaw epidermis (taken from the same animal at different locations) with EGFP fluorescence representing areas of shRNA-mediated NGF downregulation. TrkA axons contacting EGFP-positive areas are straighter (arrowheads) compared with axons in remote areas. Color images show EGFP (green) and TrkA (magenta).

(D) Curviness indexes of WT (top) and R3KO (bottom) axons within ("within EGFP area") or outside ("outside EGFP area") EGFP-positive areas. EGFP delineates areas transfected with either control or NGF shRNA. Left four panels: each line representing a difference in the average curviness index between the two areas of one animal. **$p < 0.01$; ns, not significant; paired *t* test. Right four panels: scatterplots in which each dot represents the curviness index of a single axon segment. The numbers in parentheses indicate the numbers of axon segments analyzed.

See also Figure S4.

straighter axons in WT mice. We interpreted this phenotype as an axon guidance defect and proposed that the abnormality is due to the axons' inability to respond properly to the level of NGF in the epidermis. Further experiments showed that downregulating NGF levels can ameliorate the defect in R3KO mice. This is most likely because lower NGF levels match the sensitivity range of hypersensitive IP_3Rs in R3KO growth cones such that R3KO axons are guided correctly to their targets. These findings strongly support our model that, depending on the involvement of IP_3R3, growth cones respond to different concentration ranges of IP_3-based guidance signals.

In conclusion, we identified IP_3R3 as an important subunit in keeping the sensitivity of functional IP_3R within a range that matches the availability of IP_3-based guidance cues in the environment. This IP_3R3-based sensitivity regulation is necessary for the production of asymmetric Ca^{2+} signals in DRG growth cones exposed to different concentration ranges of NGF. Other types of axons should also navigate long distances during development through different segments along the chemical gradient of guidance cues and therefore be equipped with similar machineries for sensitivity adjustment. Future studies should address the broader verification of IP_3R subtype-dependent regulation of growth cone sensitivity in developing and regenerating axons.

Limitations of the Study

Although this paper showed that IP_3R3 regulates growth cone sensitivity to IP_3-based guidance signals such as NGF, it remains unclear how this IP_3R3-dependent adjustment can be tuned during axonal navigation *in vivo*. Because each WT axon follows a well-organized and almost straight trajectory toward the epidermis in spite of varying expression levels of NGF (Figures 7 and 8), this system may be suitable for investigating mechanisms underlying IP_3R3-dependent tuning of axon guidance *in vivo*. Further studies are needed to monitor NGF downstream signaling in individual axons such as TrkA phosphorylation and to investigate its causative relationship with regulated expression and/or activity of IP_3R3.

METHODS

All methods can be found in the accompanying Transparent Methods supplemental file.

SUPPLEMENTAL INFORMATION

Supplemental Information can be found online at https://doi.org/10.1016/j.isci.2020.100963.

ACKNOWLEDGMENTS

This work was supported by Grant-in-Aid for Scientific Research B 19H03332 and AMED-CREST JP18gm0910006 to H.K. and Japan Society for the Promotion of Science International Fellowship to C.C. We are grateful to Y. Takahashi for the Tol2 vectors. We thank our laboratory members, T. Hida and H. Ito, for their assistance with this research, A.T. Guy for critical reading of this manuscript, and the RIKEN Center for Brain Science's Research Resources Division for experimental instruments.

AUTHOR CONTRIBUTIONS

C.C. performed the experiments in Figures 1, 2, 3, 4, 5, 6, 7, 8, and S1–S3 and wrote the manuscript. N.O. performed the experiments in Figures 4, 8, and S4. H.A. contributed to Figures 1, 2, 3, and 4. T.F. provided axon growth data in the manuscript. M.I. performed the experiments in Videos S1 and S2. T.M. and K.M. designed and generated IRIS2.3. T.S. provided guidance for Figure 8. H.K. designed the research project, directed the experiments, and wrote the manuscript with C.C.

DECLARATION OF INTERESTS

The authors declare no competing interests.

Received: August 30, 2019
Revised: February 10, 2020
Accepted: February 29, 2020
Published: March 27, 2020

REFERENCES

Akiyama, H., and Kamiguchi, H. (2010). Phosphatidylinositol 3-kinase facilitates microtubule-dependent membrane transport for neuronal growth cone guidance. J. Biol. Chem. *285*, 41740–41748.

Akiyama, H., Matsu-ura, T., Mikoshiba, K., and Kamiguchi, H. (2009). Control of neuronal growth cone navigation by asymmetric inositol 1,4,5-trisphosphate signals. Sci. Signal. *2*, ra34.

Albers, K.M., Wright, D.E., and Davis, B.M. (1994). Overexpression of nerve growth factor in epidermis of transgenic mice causes hypertrophy of the peripheral nervous system. J. Neurosci. *14*, 1422–1432.

Bentley, D., and Toroian-Raymond, A. (1986). Disoriented pathfinding by pioneer neurone growth cones deprived of filopodia by cytochalasin treatment. Nature *323*, 712–715.

Blondel, O., Takeda, J., Janssen, H., Seino, S., and Bell, G.I. (1993). Sequence and functional characterization of a third inositol trisphosphate receptor subtype, IP_3R-3, expressed in pancreatic islets, kidney, gastrointestinal tract, and other tissues. J. Biol. Chem. *268*, 11356–11363.

Botchkarev, V.A., Yaar, M., Peters, E.M., Raychaudhuri, S.P., Botchkareva, N.V., Marconi, A., Raychaudhuri, S.K., Paus, R., and Pincelli, C. (2006). Neurotrophins in skin biology and pathology. J. Invest. Dermatol. *126*, 1719–1727.

Chaloux, B., Caron, A.Z., and Guillemette, G. (2007). Protein kinase A increases the binding affinity and the Ca^{2+} release activity of the inositol 1,4,5-trisphosphate receptor type 3 in RINm5F cells. Biol. Cell *99*, 379–388.

Dyer, J.L., Mobasheri, H., Lea, E.J.A., Dawson, A.P., and Michelangeli, F. (2003). Differential effect of PKA on the Ca^{2+} release kinetics of the type I and III $InsP_3$ receptors. Biochem. Biophys. Res. Commun. *302*, 121–126.

Enriquez-Barreto, L., Palazzetti, C., Brennaman, L.H., Maness, P.F., and Fairen, A. (2012). Neural cell adhesion molecule, NCAM, regulates thalamocortical axon pathfinding and the organization of the cortical somatosensory representation in mouse. Front. Mol. Neurosci. *5*, 76.

Furuichi, T., Yoshikawa, S., Miyawaki, A., Wada, K., Maeda, N., and Mikoshiba, K. (1989). Primary structure and functional expression of the inositol 1,4,5-trisphosphate-binding protein P400. Nature *342*, 32–38.

Gallo, G., Lefcort, F.B., and Letourneau, P.C. (1997). The trkA receptor mediates growth cone turning toward a localized source of nerve growth factor. J. Neurosci. *17*, 5445–5454.

Gallo, G., and Letourneau, P. (2002). Axon guidance: proteins turnover in turning growth cones. Curr. Biol. *12*, R560–R562.

Giovannucci, D.R., Groblewski, G.E., Sneyd, J., and Yule, D.I. (2000). Targeted phosphorylation of inositol 1,4,5-trisphosphate receptors selectively inhibits localized Ca^{2+} release and shapes oscillatory Ca^{2+} signals. J. Biol. Chem. *275*, 33704–33711.

Gomez, T.M., and Zheng, J.Q. (2006). The molecular basis for calcium-dependent axon pathfinding. Nat. Rev. Neurosci. *7*, 115–125.

Henley, J.R., Huang, K.H., Wang, D., and Poo, M.M. (2004). Calcium mediates bidirectional growth cone turning induced by myelin-associated glycoprotein. Neuron *44*, 909–916.

Honig, M.G., Camilli, S.J., and Xue, Q.S. (2002). Effects of L1 blockade on sensory axon outgrowth and pathfinding in the chick hindlimb. Dev. Biol. *243*, 137–154.

Hu, X., Cai, J., Yang, J., and Smith, G.M. (2010). Sensory axon targeting is increased by NGF gene therapy within the lesioned adult femoral nerve. Exp. Neurol. *223*, 153–165.

Iwai, M., Tateishi, Y., Hattori, M., Mizutani, A., Nakamura, T., Futatsugi, A., Inoue, T., Furuichi, T., Michikawa, T., and Mikoshiba, K. (2005). Molecular cloning of mouse type 2 and type 3 inositol 1,4,5-trisphosphate receptors and identification of a novel type 2 receptor splice variant. J. Biol. Chem. *280*, 10305–10317.

Lohof, A.M., Quillan, M., Dan, Y., and Poo, M.M. (1992). Asymmetric modulation of cytosolic cAMP activity induces growth cone turning. J. Neurosci. *12*, 1253–1261.

Maes, K., Missiaen, L., Parys, J.B., De Smet, P., Sienaert, I., Waelkens, E., Callewaert, G., and De Smedt, H. (2001). Mapping of the ATP-binding sites on inositol 1,4,5-trisphosphate receptor type 1 and type 3 homotetramers by controlled proteolysis and photoaffinity labeling. J. Biol. Chem. *276*, 3492–3497.

Matsu-ura, T., Shirakawa, H., Suzuki, K.G.N., Miyamoto, A., Sugiura, K., Michikawa, T., Kusumi, A., and Mikoshiba, K. (2019). Dual-FRET imaging of IP_3 and Ca^{2+} revealed Ca^{2+}-induced IP_3 production maintains long lasting Ca^{2+} oscillations in fertilized mouse eggs. Sci. Rep. *9*, 4829.

Mikoshiba, K. (2007). IP_3 receptor/Ca^{2+} channel: from discovery to new signaling concepts. J. Neurochem. *102*, 1426–1446.

Ming, G., Song, H., Berninger, B., Inagaki, N., Tessier-Lavigne, M., and Poo, M. (1999). Phospholipase C-gamma and phosphoinositide 3-kinase mediate cytoplasmic signaling in nerve growth cone guidance. Neuron *23*, 139–148.

Ming, G.L., Wong, S.T., Henley, J., Yuan, X.B., Song, H.J., Spitzer, N.C., and Poo, M.M. (2002). Adaptation in the chemotactic guidance of nerve growth cones. Nature *417*, 411–418.

Miyakawa, T., Maeda, A., Yamazawa, T., Hirose, K., Kurosaki, T., and Iino, M. (1999). Encoding of Ca^{2+} signals by differential expression of IP_3 receptor subtypes. EMBO J. *18*, 1303–1308.

Monkawa, T., Miyawaki, A., Sugiyama, T., Yoneshima, H., Yamamoto-Hino, M., Furuichi, T., Saruta, T., Hasegawa, M., and Mikoshiba, K. (1995). Heterotetrameric complex formation of inositol 1,4,5-trisphosphate receptor subunits. J. Biol. Chem. *270*, 14700–14704.

Nakade, S., Rhee, S.K., Hamanaka, H., and Mikoshiba, K. (1994). Cyclic AMP-dependent phosphorylation of an immunoaffinity-purified homotetrameric inositol 1,4,5-trisphosphate receptor (type I) increases Ca2+ flux in reconstituted lipid vesicles. J. Biol. Chem. *269*, 6735–6742.

Newton, C.L., Mignery, G.A., and Südhof, T.C. (1994). Co-expression in vertebrate tissues and cell lines of multiple inositol 1,4,5-trisphosphate ($InsP_3$) receptors with distinct affinities for $InsP_3$. J. Biol. Chem. *269*, 28613–28619.

Nucifora, F.C., Jr., Sharp, A.H., Milgram, S.L., and Ross, C.A. (1996). Inositol 1,4,5-trisphosphate receptors in endocrine cells: localization and association in hetero- and homotetramers. Mol. Biol. Cell *7*, 949–960.

Patel, T.D., Jackman, A., Rice, F.L., Kucera, J., and Snider, W.D. (2000). Development of sensory neurons in the absence of NGF/TrkA signaling in vivo. Neuron *25*, 345–357.

Piper, M., Salih, S., Weinl, C., Holt, C.E., and Harris, W.A. (2005). Endocytosis-dependent desensitization and protein synthesis-dependent resensitization in retinal growth cone adaptation. Nat. Neurosci. *8*, 179–186.

Rosoff, W.J., Urbach, J.S., Esrick, M.A., McAllister, R.G., Richards, L.J., and Goodhill, G.J. (2004). A new chemotaxis assay shows the extreme sensitivity of axons to molecular gradients. Nat. Neurosci. *7*, 678–682.

Shah, S.Z.A., Zhao, D., Khan, S.H., and Yang, L. (2015). Regulatory mechanisms of endoplasmic reticulum resident IP_3 receptors. J. Mol. Neurosci. *56*, 938–948.

Sharp, A.H., Nucifora, F.C., Jr., Blondel, O., Sheppard, C.A., Zhang, C., Snyder, S.H., Russell, J.T., Ryugo, D.K., and Ross, C.A. (1999). Differential cellular expression of isoforms of inositol 1,4,5-triphosphate receptors in neurons and glia in brain. J. Comp. Neurol. *406*, 207–220.

Soulsby, M.D., and Wojcikiewicz, R.J. (2007). Calcium mobilization via type III inositol 1,4,5-trisphosphate receptors is not altered by PKA-mediated phosphorylation of serines 916, 934, and 1832. Cell Calcium *42*, 261–270.

Straub, S.V., Giovannucci, D.R., Bruce, J.I., and Yule, D.I. (2002). A role for phosphorylation of inositol 1,4,5-trisphosphate receptors in defining calcium signals induced by Peptide agonists in pancreatic acinar cells. J. Biol. Chem. *277*, 31949–31956.

Südhof, T.C., Newton, C.L., Archer, B.T., 3rd, Ushkaryov, Y.A., and Mignery, G.A. (1991). Structure of a novel $InsP_3$ receptor. EMBO J. *10*, 3199–3206.

Taylor, C.W., Genazzani, A.A., and Morris, S.A. (1999). Expression of inositol trisphosphate receptors. Cell Calcium *26*, 237–251.

Tojima, T., Hines, J.H., Henley, J.R., and Kamiguchi, H. (2011). Second messengers and membrane trafficking direct and organize growth cone steering. Nat. Rev. Neurosci. *12*, 191–203.

Tojima, T., Itofusa, R., and Kamiguchi, H. (2014). Steering neuronal growth cones by shifting the

imbalance between exocytosis and endocytosis. J. Neurosci. *34*, 7165–7178.

Tucker, K.L., Meyer, M., and Barde, Y.A. (2001). Neurotrophins are required for nerve growth during development. Nat. Neurosci. *4*, 29–37.

Van Haastert, P.J., Van Driel, R., Jastorff, B., Baraniak, J., Stec, W.J., and De Wit, R.J. (1984). Competitive cAMP antagonists for cAMP-receptor proteins. J. Biol. Chem. *259*, 10020–10024.

Vanderheyden, V., Devogelaere, B., Missiaen, L., De Smedt, H., Bultynck, G., and Parys, J.B. (2009). Regulation of inositol 1,4,5-trisphosphate-induced Ca^{2+} release by reversible phosphorylation and dephosphorylation. Biochim. Biophys. Acta *1793*, 959–970.

Wang, T., Jing, X., DeBerry, J.J., Schwartz, E.S., Molliver, D.C., Albers, K.M., and Davis, B.M. (2013). Neurturin overexpression in skin enhances expression of TRPM8 in cutaneous sensory neurons and leads to behavioral sensitivity to cool and menthol. J. Neurosci. *33*, 2060–2070.

Wojcikiewicz, R.J., and He, Y. (1995). Type I, II and III inositol 1,4,5-trisphosphate receptor co-immunoprecipitation as evidence for the existence of heterotetrameric receptor complexes. Biochem. Biophys. Res.Commun. *213*, 334–341.

Wojcikiewicz, R.J., and Luo, S.G. (1998). Differences among type I, II, and III inositol-1,4,5-trisphosphate receptors in ligand-binding affinity influence the sensitivity of calcium stores to inositol-1,4,5-trisphosphate. Mol. Pharmacol. *53*, 656–662.

Xu, J., Rosoff, W.J., Urbach, J.S., and Goodhill, G.J. (2005). Adaptation is not required to explain the long-term response of axons to molecular gradients. Development *132*, 4545–4552.

Ziemba, K.S., Chaudhry, N., Rabchevsky, A.G., Jin, Y., and Smith, G.M. (2008). Targeting axon growth from neuronal transplants along preformed guidance pathways in the adult CNS. J. Neurosci. *28*, 340–348.

iScience, Volume *23*

Supplemental Information

Inositol 1,4,5-Trisphosphate Receptor Type 3 Regulates Neuronal Growth Cone Sensitivity to Guidance Signals

Carmen Chan, Noriko Ooashi, Hiroki Akiyama, Tetsuko Fukuda, Mariko Inoue, Toru Matsu-ura, Tomomi Shimogori, Katsuhiko Mikoshiba, and Hiroyuki Kamiguchi

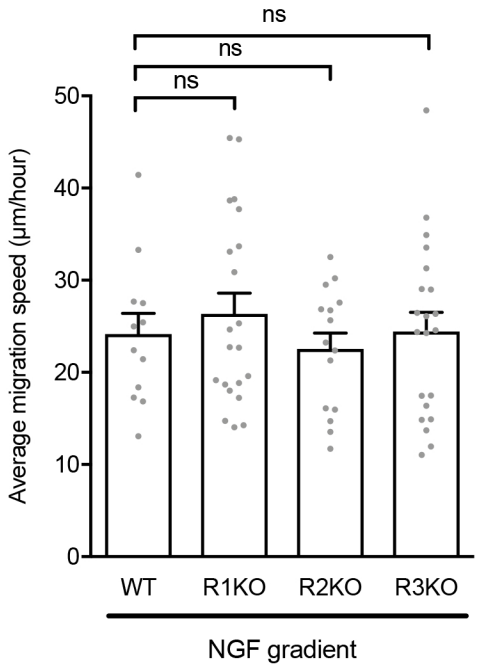

Figure S1. Growth cone migration speed in NGF gradients. Related to Figure 1.
WT and IP_3R subtype-specific knockout growth cones migrating in NGF gradients were observed under differential interference contrast microscopy, and the average displacement of the central domain distal edge was quantified and expressed as micrometers per hour. Bars represent mean ± SEM, with each gray dot indicating data from a single growth cone. ns, not significant; Dunnett's test.

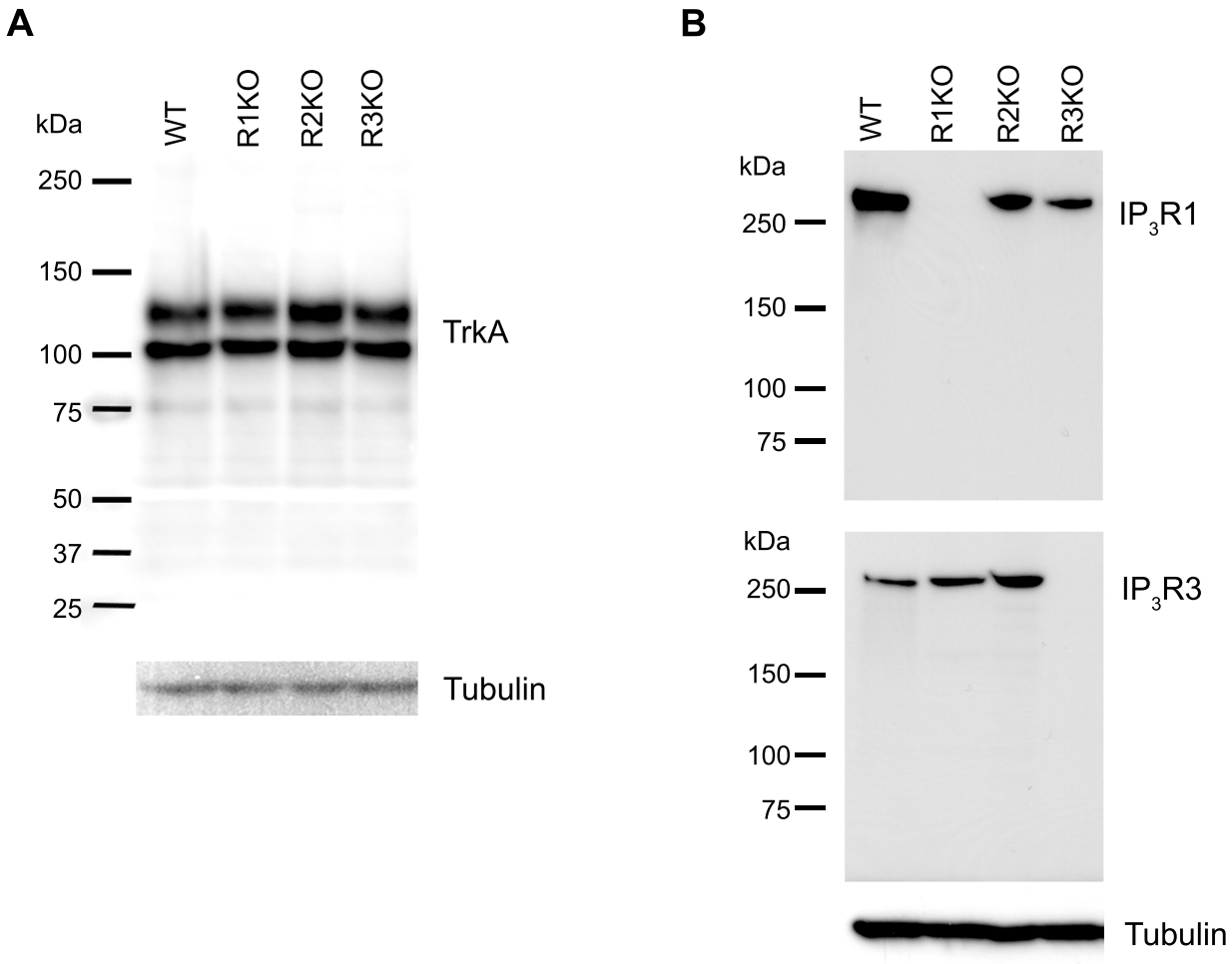

Figure S2. Western blot analysis of TrkA and IP_3R subtypes. Related to Figures 2 and 3.
(A) Shown are TrkA and tubulin (loading control) in DRGs of WT and IP_3R subtype-specific knockout mice. According to a previous report (Barker et al., 1993), the anti-TrkA antibody used here can detect both TrkA full-length protein at approximately 140 kDa and an isoform of glycosylated TrkA at approximately 110 kDa.
(B) Shown are IP_3R1, IP_3R3 and tubulin (loading control) in DRGs of WT and IP_3R subtype-specific knockout mice.

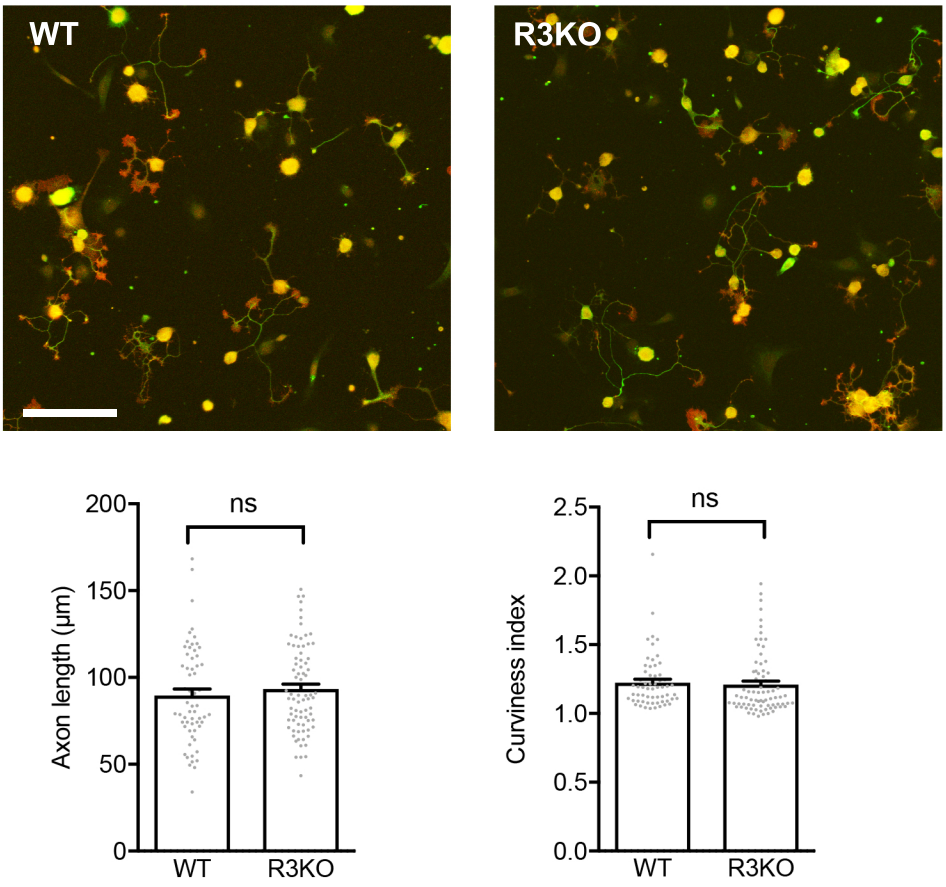

Figure S3. Directional axon growth from WT and R3KO neurons. Related to Figure 7.
WT or R3KO DRG neurons cultured on poly-D-lysine substrates for five hours were fixed and immunostained for neuronal tubulin (green) and TrkA (red). Scale bar, 100 μm. Between WT and R3KO neurons, neither axon length nor curviness index showed statistically significant difference by Student's *t* test. Numbers in brackets represent the number of axons included in each group. Data are represented as mean ± SEM.

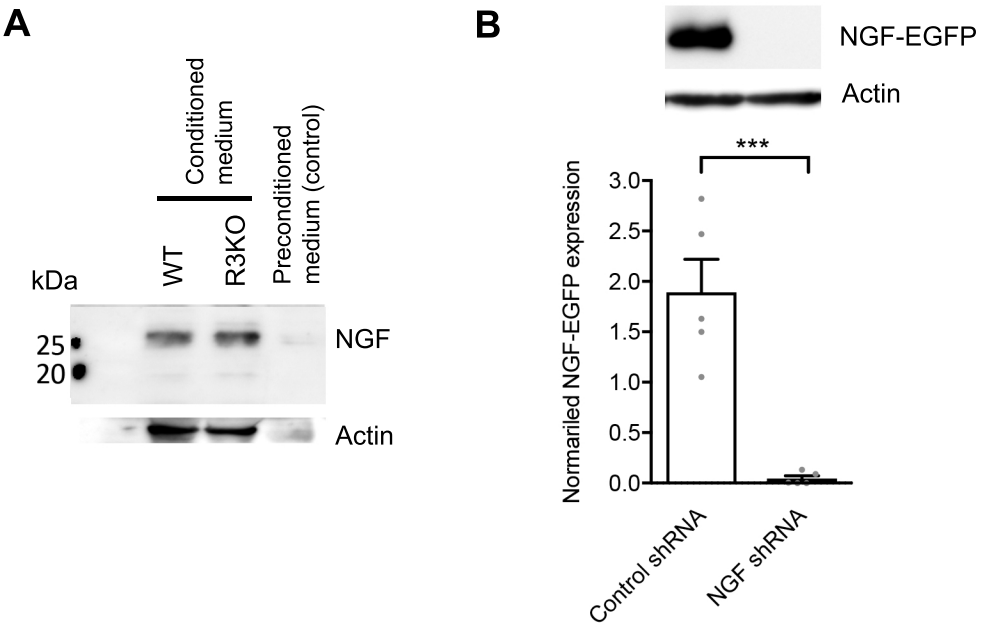

Figure S4. NGF release from keratinocytes and its downregulation by shRNA. Related to Figures 7 and 8. (A) Skin keratinocyte cultures were prepared from Wt and R3KO mice. Four days after plating, 60 mL of conditioned medium was concentrated to 200 µL using Amicon columns according to manufacturer's protocol. The concentrated medium was processed for Western blotting to detect endogenous NGF and actin as a loading control. (B) The effect of NGF shRNA on NGF expression was assessed in keratinocytes transfected with a construct coding NGF-EGFP fusion protein. NGF-EGFP expression was quantified by immunoblotting with GFP antibodies (Santa Cruz, sc-9996; 1/1000 overnight at 4°C). The graph shows NGF-EGFP normalized to actin. Bars represent mean ± SEM, with each gray dot indicating data from each of 5 independent experiments. *** $p < 0.001$; Student's *t* test.

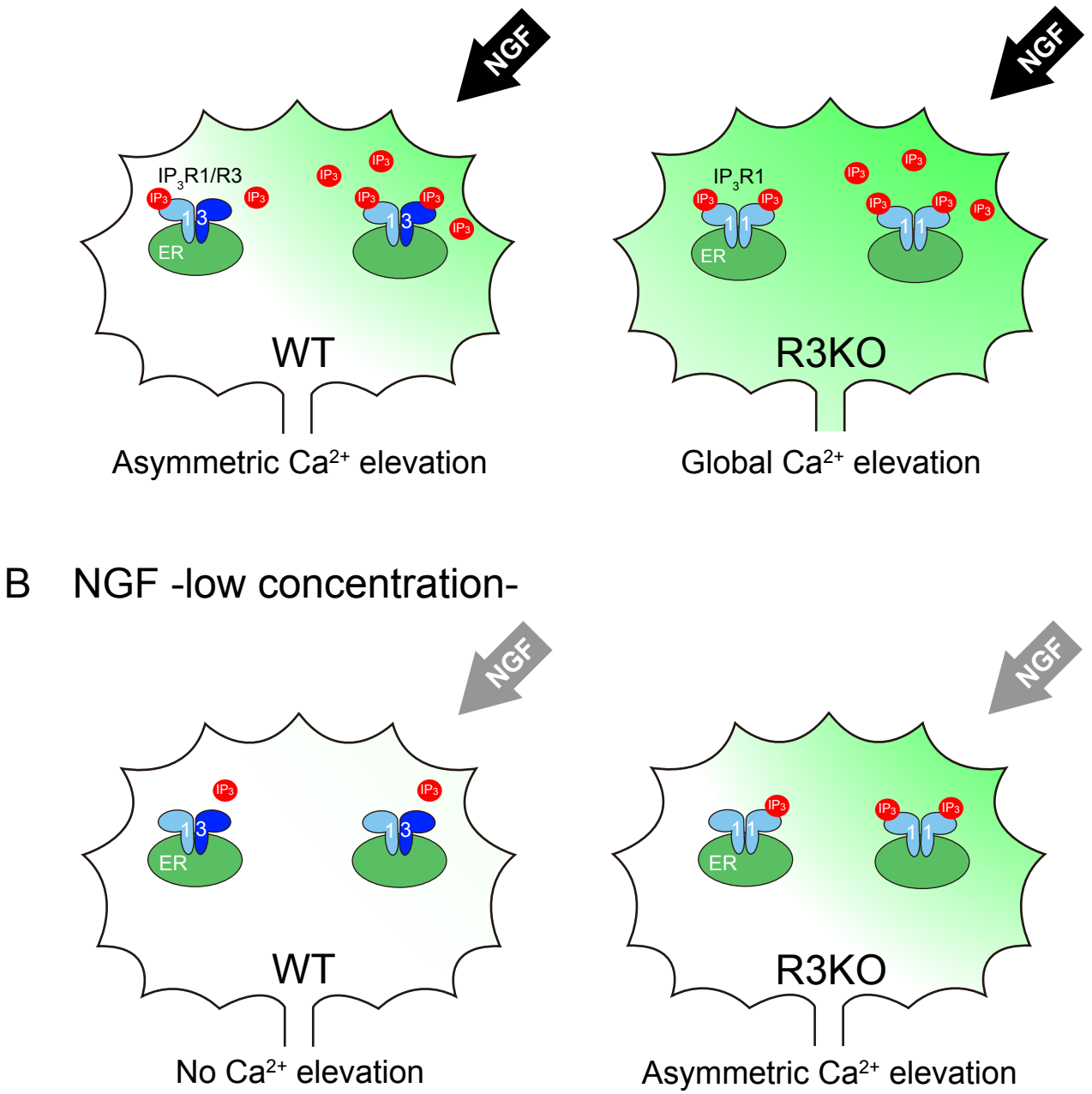

Figure S5. **Model of IP_3R3 involvement in the regulation of growth cone sensitivity to guidance signals**.
(A) An extracellular NGF gradient (arrow) evokes the production of IP_3 (red) on the near side of the growth cone. The localized IP_3 elevation in turn causes IICR (green) only on the near side of WT growth cone or on both sides of R3KO growth cone. In WT, type 3 subunit ('3') forms tetrameric IP_3Rs with relatively low IP_3 affinity. As a result, these IP_3Rs can confine IICR to the near side even in the presence of small amounts of far-side IP_3 that are produced locally or diffused from the near side. In R3KO, however, the low levels of IP_3 on the far side are above the threshold required to activate IP_3Rs that consist exclusively of the higher-affinity type 1 subunit ('1'). Such abnormal IICR on the far side abolishes Ca^{2+} signal asymmetry, therefore renders R3KO growth cones irresponsive to normal concentration ranges of NGF that can attract WT growth cones.
(B) When extracellular NGF concentration is too low, WT growth cone cannot generate Ca^{2+} signals even on the near side. Therefore, they fail to recognize such a low level of NGF as an attractive cue. By contrast, hypersensitive IP_3R in R3KO growth cone can generate IICR on the near side, and this growth cone can turn toward lower-than-threshold NGF required for WT growth cone turning.

Transparent Methods

Mice

R1KO, R2KO and R3KO mice (Futatsugi et al., 2005; Matsumoto et al., 1996) were maintained at the RIKEN Center for Brain Science Animal Care Facility. The experimental procedures and housing conditions for animals were approved by the Wako Animal Experiments Committee at RIKEN, and all of the animals were cared for and treated humanely in accordance with the Institutional Guidelines for Experiments Using Animals. Postnatal day 0 mice were used without sex determination.

Western blotting

DRGs were homogenized by sonication in lysis buffer as described (Wada et al., 2016). DRG lysate proteins were separated by SDS-PAGE and transferred to PVDF membranes (Merck Millipore). After blocking with 5% skim milk and 0.1% Tween 20 in PBS at room temperature for 1 hour, the membranes were incubated at 4°C overnight with anti-TrkA (R&D) anti-IP_3R1 (4C11; Otsu et al., 1990), anti-IP_3R3 (BD Biosciences) and anti-tubulin antibodies (Covance/Biolegend). After incubation with HRP-conjugated secondary antibodies, bands were visualized with chemiluminescent substrate solutions (Pierce™ ECL Western Blotting Substrate; Thermo Fisher Scientific). For immunoblotting of multiple IP_3R subtypes, the membranes were stripped with stripping buffer (Restore™ Western Blot Stripping Buffer; Thermo Fisher Scientific) before incubation with a different primary antibody.

Cell culture

DRGs dissected from postnatal day 0 mice were dissociated and plated on a glass-based dish coated with poly-D-lysine and 10 μg/ml laminin (Life Technologies). The cells were incubated at 37°C in RPMI-1640 medium (Invitrogen) supplemented with 10% fetal bovine serum and 10 ng/ml NGF (Promega) for 2 hours. The medium was then changed to serum-free Neurobasal®-A (Invitrogen) supplemented with B-27 (Invitrogen) before starting experiments.

Growth cone turning assay

Assays of growth cone turning induced by FLIP of caged IP_3 were performed as described previously (Akiyama et al., 2009). Briefly, DRG neurons were loaded with a caged IP_3 derivative (iso-Ins(1,4,5)P_3/PM; 0.5 μM or 0.1 μM in media; Alexis Biochemicals) and 0.02% Cremophor EL (Sigma-Aldrich) in L15 medium (Life Technologies) for 30 min and then washed with L15 alone. Afterwards the cells were incubated with NGF-containing L15 for at least 30 min before the start of experiments. Spatially restricted IP_3 signals were generated by repetitive FLIP every three seconds. Differential interference contrast images of growth cones were acquired before and up to 30 min after the start of repetitive FLIP.

Assays of growth cone turning induced by a microscopic gradient of NGF (0.025 to 50 μg/ml in pipette) or MAG (150 μg/ml in pipette; R&D systems) were performed as described previously (Hong et al., 2000; Lohof et al., 1992). The gradient was produced by pulsatile pressure ejection of NGF or MAG from a micropipette positioned at a 45° angle 100 μm from the growth cone. The turning angle was defined as the difference in growth cone migration direction before and 40 minutes after the start of pulsatile ejection of guidance molecules.

Ca^{2+} imaging

For imaging IP_3-induced Ca^{2+} elevations, we used the fluorescent Ca^{2+} indicator Fluo-8H (4μM, AAT Bioquest). For quantitative analysis, two ROIs were positioned on each growth cone: the near side ROI defined as a circular region whose center corresponded to the site of laser irradiation and whose diameter equaled to one-third of the width of each growth cone; the far side ROI defined as a circular region of the same diameter that was placed on the center of the far-side half of each growth cone. The averaged Fluo-8H fluorescence intensity within each ROI (F) at each time point was normalized to the baseline Fluo-8H intensity (F_{base}), the averaged F before the onset of FLIP of IP_3. Then, the ratio F/F_{base} (defined as F') was used as a measure of cytosolic Ca^{2+} signals.

For imaging NGF-induced Ca^{2+} elevations, DRG neurons were preloaded with a ratiometric pair of calcium indicators, OGB-1-AM (2 μM, Invitrogen) and FR-AM (2.5 μM, Invitrogen), as described previously (Akiyama et al., 2009). Within each ROI on a growth cone, the emission ratio ($F_{OGB\text{-}1}/F_{FR}$, defined as R) was normalized to the baseline value (defined as R_{base}), and R/R_{base} (defined as R') was used a measure of cytosolic Ca^{2+} signals.

IP_3 imaging

Neurons were transfected with the IRIS-2.3 construct (Matsu-ura et al., 2019) using Nucleofector (Lonza) according to the manufacturer's protocols. The donor (EGFP) of IRIS-2.3 was excited with 488 nm light, and fluorescence images of EGFP and HaloTag®-TMR were acquired simultaneously with a CCD camera (ImagEM, Hamamatsu Photonics) after the dual-color image was split with an emission splitter. Because FRET efficiency from EGFP to HaloTag®-TMR decreases on IP_3 binding to IRIS-2.3, we calculated the inverse FRET ratio, i.e., the ratio of EGFP emission compared to TMR emission (F_{EGFP}/F_{TMR}, defined as R_{FRET}). Within each ROI, the averaged R_{FRET} was normalized to the baseline value (defined as $R_{FRET\text{-}base}$), and $R_{FRET}/R_{FRET\text{-}base}$ (defined as R') was used a measure of IP_3 levels.

Immunohistochemistry

The hindpaws of postnatal day 0 mice were collected in ice-cold PBS and fixed in 4% paraformaldehyde overnight. Tissue sections were made on a vibratome at 40 μm thickness and collected in regular PBS. From the blocking step onwards, high saline buffer (HSB: 500 mM

NaCl, 9.2 mM NaH_2PO_4, 12.5 mM Na_2HPO_4) was used to minimize background staining (Ramos-Vara, 2005). The sections were incubated overnight at 4ºC with primary antibodies against NGF (polyclonal rabbit, 1/500; EMD Millipore/Chemicon), TrkA (polyclonal goat, 1/100; R&D), GFP (monoclonal rat, 1/2000; Nacalai Tesque). On the next day, the sections were incubated in Alexa Fluor dye-conjugated secondary antibodies (1/500; Molecular Probes/ThermoFisher).

Whole-mount immunofluorescence and three-dimensional reconstruction

The hindpaw planta of postnatal day 0 mice were stained and tissue cleared according to the iDISCO method (Renier et al., 2014; Takahashi et al., 2019) with some modifications. In brief, the tissue was fixed in 4% paraformaldehyde overnight, treated with methanol, blocked with normal horse serum and incubated with anti-rat TrkA (polyclonal goat, 1/100; R&D) and a secondary antibody conjugated with Alexa Fluor 594 (1/1000; Molecular Probes/ThermoFisher). The specimen was imaged using a 63x HC PL APO CS2 oil immersion objective lens on a TCS SP8 confocal microscope (Leica Microsystems) controlled by LASX software. Three-dimensional animations were constructed from captured image stacks using LASX software.

NGF knockdown

We used RNA interference to knock down NGF expression in the skin. The 29-mer shRNA targeted against the ngf gene was purchased from Origene (catalog# TG510273). The 29-mer shRNA against turbo-red fluorescence protein (tRFP; catalog#TR30017) was used as a negative control. The NGF-targeting sequence was 5'-TGTGCTCAGCAGGAAGGCTACAAGAAGAG-3'. The negative control sequence was 5'-CTTCAAGACCACATACAGATCCAAGAAAC-3'. The shRNA cassette containing the U6 promoter, the shRNA hairpin and the termination sequence (TTTTTT) was sub-cloned into the tol2 plasmid (kind gift from Dr. Y. Takahashi, Kyoto University, Japan) (Sato et al., 2007). This is a transposon-donor plasmid harboring the Tol2 construct containing the CAG promoter and EGFP gene. Cotransfection with the transposase plasmid allowed long-term expression of NGF shRNA.

The effect of NGF knockdown was confirmed in primary cultures of skin keratinocytes transfected with the tol2 plasmid for NGF-EGFP expression. The plasmid encodes for a protein, in which NGF in its N-terminus is fused with EGFP via a linker sequence of ADPPVAT.

The shRNA plasmids were delivered into hindpaw skin epidermal cells via *in utero* electroporation, using previously established methods (Chan et al., 2019; Fukuchi-Shimogori and Grove, 2001; Matsui et al., 2011) with modifications for skin transfection. Briefly, a pregnant mouse was anesthetized with medetomidine, midazolam, and butorphanol. For each embryo (embryonic day 13 to 14), a mixture of 1 µl of 3 µg/µl shRNA plasmid and 1 µl of 1 µg/µl transposase plasmid was injected into the intra-amniotic space between the body and the right

hindpaw. Immediately, the embryo was electroporated using a protocol recommended by the manufacturer (Nepa Gene). The positive pole of pad platinum electrodes was placed on the dorsal surface of embryo's right hindpaw, and the negative pole on the left side of its body. Then, square pulses of 45-V amplitude and 50-ms pulse duration were administrated.

Quantification of axon morphology

To compare WT and R3KO TrkA axon morphologies, axons residing in the medial hind paw just caudal to the walking pad were included in the quantification. This is because axon morphologies in this region are the most consistent across animals. For quantification on a confocal microscopic image, we first defined the start and end points of each axon segment to be included in the analysis. The start was defined as the point where an axon crosses the boundary between the epidermal basal layer and the stratum spinosum that can be easily identified by NGF immunofluorescence. The end was defined as the distal tip of that axon. Then, we measured the length of each axon segment and the straight-line distance between the two ends of that segment, using the NeuronJ Plugin in ImageJ (Meijering et al., 2004). Axon morphologies were represented by the curviness index that was defined as the segment length divided by the linear distance between the two ends of that segment.

In experiments designed to examine the effect of NGF downregulation on the curviness index of TrkA axons, an epidermal area containing a cluster of more than three EGFP-positive cells was defined as an EGFP-positive area. Axons coursing within or in direct contact with this area were categorized as those 'within EGFP area'. For comparison, equal numbers of axons on each outside of the EGFP-positive area were categorized as those 'outside EGFP area'. For example, when three axons were found within EGFP area, three axons on the left and three axons on the right in the immediate neighborhood were included in the category of axons outside EGFP area, giving 3 test readings and 6 control readings of the curviness index.

Selection of axons and determination of the curviness index were performed by a researcher who was blind to mouse genotypes and treatment conditions.

Statistical analysis

All data are expressed as the mean ± SEM. Statistical analysis was performed using GraphPad Prism 7 (GraphPad Software). Each dataset was tested for normality by D'Agostino and Pearson omnibus or Shapiro-Wilk test. For analysis between two groups, normally distributed data were tested for equality of variances by F-test followed by paired *t* test or student's *t* test. Non-normally distributed data were analyzed by Wilcoxon matched pairs signed rank test. For analysis of three or more groups, normally distributed data were analyzed by Dunnett's multiple comparison test. All tests were two-tailed, and $P < 0.05$ was considered to be statistically significant.

Supplemental References

Barker, P.A., Lomen-Hoerth, C., Gensch, E.M., Meakin, S.O., Glass, D.J., Shooter, E.M. (1993). Tissue-specific alternative splicing generates two isoforms of the trkA receptor. J Biol Chem *268*,15150-15157.

Chan, C., Kamiguchi, H., and Shimogori, T. (2019). Spatially restricted long-term transgene expression in the developing skin used for studying the interaction of epidermal development and sensory innervation. Dev Growth Differ *61*, 276-282.

Fukuchi-Shimogori, T., and Grove, E.A. (2001). Neocortex patterning by the secreted signaling molecule FGF8. Science *294*, 1071-1074.

Futatsugi, A., Nakamura, T., Yamada, M.K., Ebisui, E., Nakamura, K., Uchida, K., Kitaguchi, T., Takahashi-Iwanaga, H., Noda, T., Aruga, J.*, et al.* (2005). IP_3 receptor types 2 and 3 mediate exocrine secretion underlying energy metabolism. Science *309*, 2232-2234.

Hong, K., Nishiyama, M., Henley, J., Tessier-Lavigne, M., and Poo, M. (2000). Calcium signalling in the guidance of nerve growth by netrin-1. Nature *403*, 93-98.

Matsui, A., Yoshida, A.C., Kubota, M., Ogawa, M., and Shimogori, T. (2011). Mouse in utero electroporation: controlled spatiotemporal gene transfection. J Vis Exp.

Matsumoto, M., Nakagawa, T., Inoue, T., Nagata, E., Tanaka, K., Takano, H., Minowa, O., Kuno, J., Sakakibara, S., Yamada, M.*, et al.* (1996). Ataxia and epileptic seizures in mice lacking type 1 inositol 1,4,5-trisphosphate receptor. Nature *379*, 168-171.

Meijering, E., Jacob, M., Sarria, J.C., Steiner, P., Hirling, H., and Unser, M. (2004). Design and validation of a tool for neurite tracing and analysis in fluorescence microscopy images. Cytometry A *58*, 167-176.

Otsu, H., Yamamoto, A., Maeda, N., Mikoshiba, K., and Tashiro, Y. (1990). Immunogold localization of inositol 1, 4, 5-trisphosphate ($InsP_3$) receptor in mouse cerebellar Purkinje cells using three monoclonal antibodies. Cell Struct Funct *15*, 163-173.

Ramos-Vara, J.A. (2005). Technical aspects of immunohistochemistry. Vet Pathol *42*, 405-426.

Renier, N., Wu, Z., Simon, D.J., Yang, J., Ariel, P., and Tessier-Lavigne, M. (2014). iDISCO: a simple, rapid method to immunolabel large tissue samples for volume imaging. Cell *159*, 896-910.

Sato, Y., Kasai, T., Nakagawa, S., Tanabe, K., Watanabe, T., Kawakami, K., and Takahashi, Y. (2007). Stable integration and conditional expression of electroporated transgenes in chicken embryos. Dev Biol *305*, 616-624.

Takahashi, S., Ishida, A., Kubo, A., Kawasaki, H., Ochiai, S., Nakayama, M., Koseki, H., Amagai, M., and Okada, T. (2019). Homeostatic pruning and activity of epidermal nerves are dysregulated in barrier-impaired skin during chronic itch development. Sci Rep *9*, 8625.

Wada, F., Nakata, A., Tatsu, Y., Ooashi, N., Fukuda, T., Nabetani, T., and Kamiguchi, H. (2016). Myosin Va and Endoplasmic Reticulum Calcium Channel Complex Regulates Membrane Export during Axon Guidance. Cell Rep *15*, 1329-1344.